

Final report

**ADVANCED MODELLING OF PIEZOCONE PENETRATION TEST USING
CAVITY EXPANSION THEORY AND INTERPRETATION SIMULATOR
DEVELOPMENT**

by

Shengli Chen

Assistant Professor

and

Kai Liu

Graduate Research Assistant

Transportation Innovation for Research Exploration Program

Grant No. DOTLT1000135

Louisiana State University

Baton Rouge, Louisiana

January, 2018

ABSTRACT

The piezocone penetration test (CPTu) is a well-established and efficient tool used in geotechnical engineering for measuring/interpreting the fundamental soil properties. However, the currently used interpretation methods for the CPTu test are largely empirical in nature and/or often based on over simplistic formulations, thus lacking the analytical rigor from the theoretical point of view. The report develops a rigorous analytical solution for the spherical cavity expansion in critical state clayey soils (i.e., modified Cam Clay soil model), which, in combination with the already existing solution for the cylindrical expansion, can and have been used here as the theoretical basis for relating the measured cone resistance, pore water pressure, and sleeve friction to the mechanical soil properties of clay deposits.

A rigorous interpretation model, on leverage of the essentially explicit expressions for the ultimate effective radial stresses at cavity wall pertaining to the spherical and cylindrical expansions, has been subsequently proposed to back calculate the desirable soil parameters including OCR (overconsolidation ratio), M (slope of the critical state line, associated with the friction angle of soil), and s_u (soil strength). As illustrative examples, the available CPTu data from two testing sites have been interpreted by using the proposed interpretation model. The results indicate that for both Brent and Grangemouth sites considered, the predicted OCR values from CPTu tests in general fit well with those from the independent oedometer tests. It is also found that the interpretation model provides reasonably well estimates of the effective internal friction angle ϕ' (within the value range of the corresponding oedometer test results) for the Grangemouth site, though its predictions on ϕ' for the Brent site are less successful. These comparative studies of

the predicted parameters from CPTu and the results obtained by other laboratory means affirm the general validity of the proposed interpretation approach.

To facilitate the applications of the above-mentioned interpretation method, an efficient simulation tool has been eventually compiled based on the Mathematica software package, and brief instructions for the use of the simulator also been presented. Such a simulator possess the advantages over the conventional ones currently in use in that it is capable of extracting maximum benefit from the CPTu data (combining all the measurements of piezocone test) and of estimating the essential geotechnical parameters as rigorous and precise as possible. It thus will benefit the site investigation in geotechnical engineering through improving the accuracy of the current interpretation technique in relevant to the CPTu tests.

ACKNOWLEDGEMENTS

The investigators appreciate the Louisiana Transportation Research Center (LTRC) for funding this project through the Transportation Innovation for Research Exploration (TIRE) Program. The authors would like to acknowledge the help, guidance, and administrative direction provided to them by Dr. Vijaya (VJ) Gopu, Associate Director of LTRC. The authors are also grateful to Dr. Lin Li for his assistance and comments during the preparation of this final report.

RESEARCH IMPLEMENTATIONS

A rigorous analytical solution for the spherical cavity expansion in modified Cam Clay soils has been developed. This newly developed cavity expansion solution, along with the already existing one for the cylindrical expansion, can and have been used in this research project as the theoretical basis for relating the measured cone resistance, pore water pressure, and sleeve friction to the mechanical soil properties of clay deposits. The outcomes of these analytical relationships, given their explicit nature, make it feasible to further establish an appropriate interpretation model for the CPTu test, and consequent development of an interpretation simulator based on the Mathematica software for practical use. The proposed model/simulator possess the advantages over the conventional ones currently in use in that it is capable of extracting maximum benefit from the CPTu data and of estimating the essential geotechnical parameters as rigorous and precise as possible. It thus will benefit the site investigation in geotechnical engineering through improving the accuracy of the current interpretation technique in relevant to the CPTu tests.

TABLE OF CONTENTS

ABSTRACT	iii
ACKNOWLEDGEMENTS	vi
RESEARCH IMPLEMENTATIONS	viii
TABLE OF CONTENTS	x
LIST OF FIGURES	xiii
CHAPTER 1. INTRODUCTION	1
1.1. Literature review	1
1.2. Statement of Problem	5
1.3. Geological Environment	7
1.4. Important Statements	7
1.5. Objective of Research	9
1.6. Report Outline	9
CHAPTER 2. ANALYSIS OF CPTU TEST USING SPHERICAL CAVITY THEORY	11
2.1. Elastic Analysis	12
2.2. Elastoplastic Analysis	13
2.3. Boundary Value Problem	18
2.4. Stress Components at Failure State	19
2.5. Summary	21
CHAPTER 3. ANALYSIS OF CPTU TEST USING CYLINDRICAL CAVITY THEORY	22
3.1. Elastic Analysis	22
3.2. Elastoplastic Analysis	23
3.3. Boundary Value Problem	26
3.4. Stress Components at Failure State	26
3.5. Summary	27
CHAPTER 4. INTERPRETATION OF CPTU TEST	29

4.1. CPTu Test and Measurement Corrections	30
4.1.1. Correction of Cone Tip Resistance q_c (Chen B.S., 1994)	30
4.1.2. Correction of Sleeve Friction f_s (Chen B.S., 1994)	32
4.2. Interpretation Method	32
4.2.1. Determination of Undrained Shear Strength s_u, s	33
4.2.2. Determination of Slope of Critical State Line M	34
4.2.3. Determination of Overconsolidation Ratio OCR	34
4.3. Case Study	35
4.3.1. CPTu Test at Brent	35
4.3.2. CPTu Test at Grangemouth	39
4.4. Summary	42
CHAPTER 5. DEVELOPMENT OF INTERPRETATION SIMULATOR	44
5.1. Overview	44
5.2. Mathematica Introduction	44
5.3. Program Usage	45
5.4. Summary	50
CHAPTER 6. CONCLUDING REMARKS	51
6.1. Conclusions	51
6.2. Suggestions and Further Research	52
REFERENCES	54
APPENDIX	58
OUTCOMES	68

LIST OF FIGURES

Fig. 1. Schematic illustration of CPTu test	2
Fig. 2. Various types of piezocone penetrometer (after Chen, B.S., 1994)	2
Fig. 3. Unequal end area of electric cone used for correcting qc and fs (after Chen B.S., 1994)	3
Fig. 4. Schematic of cavity expansion in anisotropic Cam Clay soil (Cylindrical)	6
Fig. 5. Spherical Coordinate System	11
Fig. 6. Schematic illustration of CPTu device	29
Fig. 7. Unequal end area of electric cone used for correcting qc and fs (after Chen B.S., 1994)	31
Fig. 8. Schematic illustration of mechanical equilibrium of cone face	31
Fig.9. Typical Piezocone Profiles at Brent (after Powell et al., 1988)	36
Fig. 10. Variation of OCR with depth	37
Fig.11. Variation of effective internal friction angle with depth	38
Fig.12. Typical Piezocone Profiles at Grangemouth (after Powell et al., 1988)	40
Fig. 13. Variation of OCR with depth	41
Fig. 14. Variation of effective internal friction angle with depth	42
Fig. 15. Main interface	45
Fig. 16. Interactive interface requiring parameters of CPTu tool and other basic ones	46
Fig. 17. Interactive interface requiring field measured data	47
Fig. 18. Interactive interface filled out with parameters of CPTu tool and other basic ones	48
Fig. 19. Interactive interface with obtained properties of soil	49

CHAPTER 1. INTRODUCTION

1.1. Literature review

Piezocone is a quasi-static cone penetrometer with the capability of measuring pore water pressure in addition to cone resistance and shaft friction during a quasi-static sounding using a hydraulic pushing force (Mayne, 1991; Chang et al., 2001). Due to its operational efficiency and relative cost effectiveness, piezocone penetration test (CPTu) and consequent data interpretation have been the active research areas over the years in geotechnical engineering for routine site characterization (Cai et al., 2009; Zhang et al., 2016).

At first, the cone systems were of the mechanical type and only the measurement of cone resistance can be recorded by hand (Broms and Flodin, 1988). Later, electrical type of cone penetrometers with a sleeve, which is capable of recording the continuous measurements automatically, was developed in 1949 and became commercially available in the 1960's (DeRuiter, 1971). In 1970's, electrical cone with pore pressure measurement (CPTu) was invented (Senneset, 1974), from which three independent measurements, cone tip resistance (q_c), sleeve friction (f_s), and pore water pressure (u_{bs}), can be continuously recorded during sounding, as shown in figure 1. Nowadays, the piezocone can be generally categorized as single-element piezocone and triple-element piezocone, as shown in figure 2. Based on the position where the pore pressure will be measured, single-element piezocone can be further divided into Type 1 up to Type 4, in which the pore pressure transducer is located at the cone tip, the mid-tip, the joint of cone tip and the sleeve, and on the sleeve, respectively.

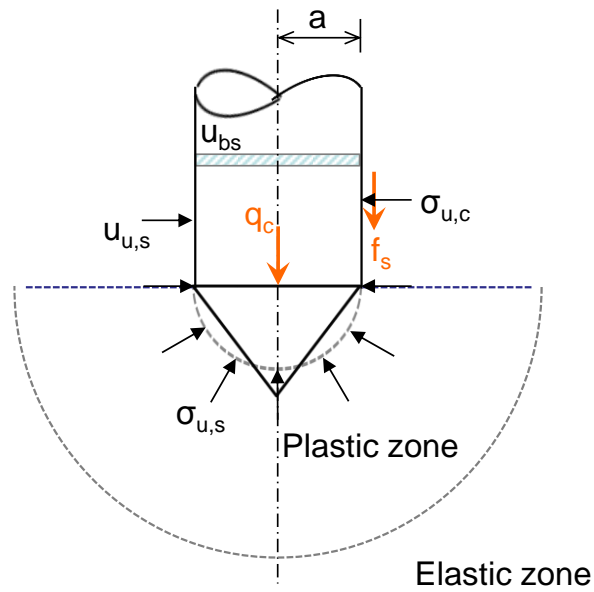


Fig. 1. Schematic illustration of CPTu test

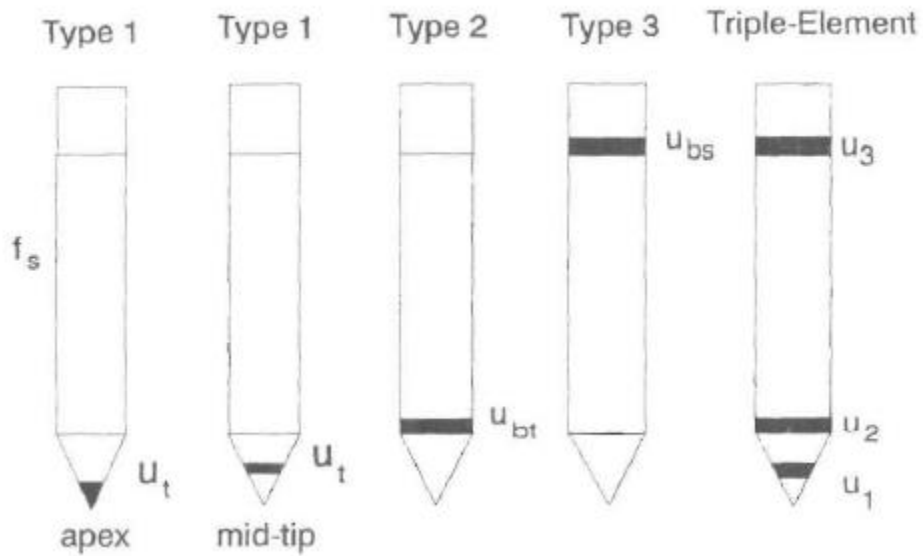


Fig. 2. Various types of piezocone penetrometer (after Chen, B.S., 1994)

It should be noted that the cone resistance q_c from Type 2 and Type 3 piezocone must be corrected for pore water pressure effects acting on unequal area projections of the cone and a correction on the sleeve friction f_s is also required if the front area is not equal in magnitude to the

end area, shown in Figure 3. Two equations are generally applied to correct the cone tip resistance q_c and the sleeve friction f_s .

$$q_t = q_c + (1 - \alpha)u_{bt} \quad (1)$$

$$f_t = f_s + \frac{A_{bs}u_{bs} - A_{bt}u_{bt}}{A_s} \quad (2)$$

where q_t is the corrected tip resistance; α , defined by $\alpha = \frac{A_n}{A_t}$, denotes the effective area ratio; u_{bt} is the pore pressure behind the tip; f_t specifies the corrected sleeve friction; A_{bt} , A_{bs} and A_s , as illustrated in Figure 3, represent the sleeve end area behind the tip, the end area behind the sleeve, and the total surface of the friction sleeve; u_{bs} and u_{bt} are the pore pressure at the corresponding location.

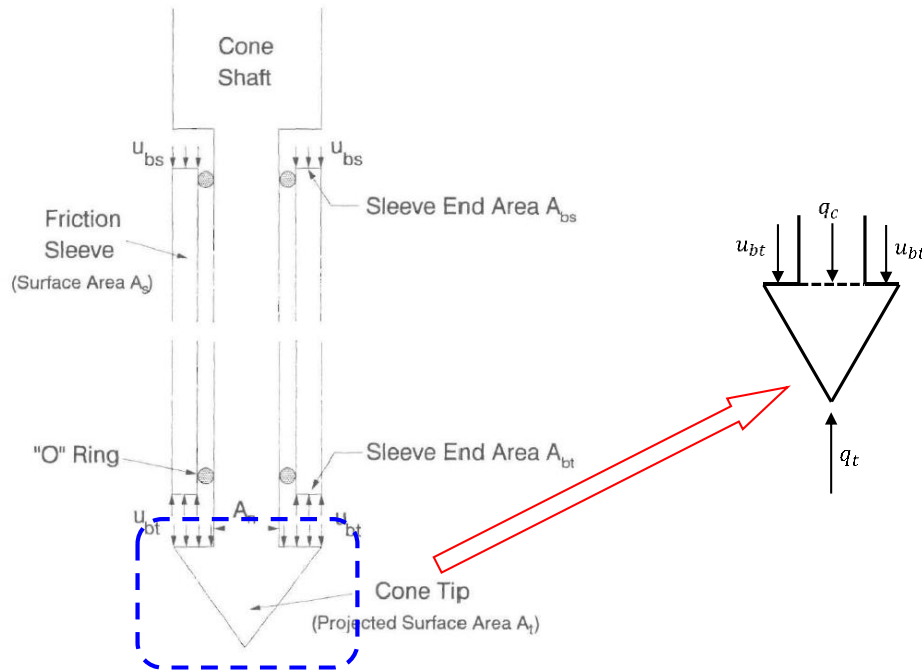


Fig. 3. Unequal end area of electric cone used for correcting q_c and f_s (after Chen B.S., 1994)

As for the interpretation methods, the results of pressuremeter tests were initially interpreted by means of empirical expressions, which are still widely used currently, to correlate the measurements with the soil properties (e.g., Schnaid 1990; Schnaid and Houlsby 1992; Eslami, Fellenius 1997; Robertson 2009; Ching 2014; Cai et al. 2009, 2017). Although these empirical approaches has been applied in interpretation of piezocone test for many years, they show poor performances in predicting the soil behavior because they are suggested merely from an empirical standpoint and are based on specific trends observed at a limited number of sites. Another disadvantage of these empirical interpretation approaches is that they were developed at specific regions and geologies, and therefore they need to be calibrated before they applied for other regions.

Although a great number of studies have contributed to proposing the correlation equations between soil properties and piezocone test results, only a few of them appear to have been derived from a theoretical standpoint due to the fact that the actual mechanism for soil failure around a penetrating cone, when involving the nonlinear plasticity deformation, is very much complicated, rendering it extremely difficult to develop a desirable analytical approach/modelling for the piezocone results evaluation. At present, the theoretical standpoints for interpretation of the piezocone test can be divided into three categories: bearing capacity theory (e.g., Durgunoglu and Mitchell 1975); the strain path theory (e.g., Baligh 1985; 1986) and the cavity expansion theory (e. g. Vesic 1972; Carter et al. 1986; Yu and Houlsby 1991; Chang et. al, 2001; Zhang et al. 2016). Compared with the latter two theories, the bearing capacity theory ignores the penetration process of the piezocone, and hence cannot yield reasonable predictions for soil properties. Moreover, although the strain path theory made some success in predicting the measurements during sounding, its complexity greatly hampers its application in back calculation of the soil properties. Among those theory standpoints, the cavity expansion theory has been successfully applied in

interpretation of piezocone measurements because the deformation mechanism of the soil around the shaft and tip of the piezocone are extremely similar to expansion of a spherical cavity and a cylindrical cavity. Mayne (1991) derived an interpretation method, by combining the spherical cavity expansion theory and modified Cam Clay model, to determine the undrained shear strength for the clay deposits. Cao et al. (2001) presented an improved solution for the undrained expansion of a cavity in modified Cam Clay soil, and the solution was further utilized to interpret the cone tip resistance, penetration pore pressure, as well as the prediction of clay properties such as s_u and OCR (Chang et al., 2001). However, none of these interpretation approaches can be considered as accurate/rigorous since they were all based on simplified and approximate formulations in obtaining the desired ultimate cavity pressure and limiting pore pressure, which results in poor performances in predicting the soil properties. Moreover, most current interpretation techniques extract the soil information only from the cone tip resistance q_c and the pore water pressure, while the sleeve friction f_s is still left unused. Hence, if all the measurements can be used simultaneously in interpretation of the piezocone test with a rigorous cavity expansion model, more soil properties can be explored and the performance of the interpretation would be greatly improved.

1.2. Statement of Problem

Teh and Houlsby (1991) showed that the penetration of a cone (Fig. 1) produced displacements quite similar to those developed during the expansion of a cavity. To be more specific, the penetration at cone face section can be modelled as the expansion of an existing spherical cavity to infinite, while the penetration at friction sleeve could be considered as the process of expanding an existing cylindrical cavity to infinite. Thus, cavity expansion theory may provide a realistic and theoretical framework for the interpretation of piezocone testing profiles.

Figure 4 schematically shows in cylindrical coordinate system the expansion of a cavity of initial radius a_0 in an infinite saturated soil subjected to an in-plane (horizontal) in situ stress σ_h and an out-of-plane (vertical) stress σ_h , as well as an initial pore pressure u_0 . Such cylindrical scenario can be written under spherical coordinate system, in which in-situ stress is still equal to σ_h and initial pore water pressure, again, holds the value of u_0 . Take cylindrical condition as an example. As internal cavity pressure increases gradually from its initial value of σ_h , yield would firstly occur at cavity wall. Plastic zone will be formed subsequently around cavity with further increase of cavity pressure. Consider the situations where cavity is expanded to the current radius

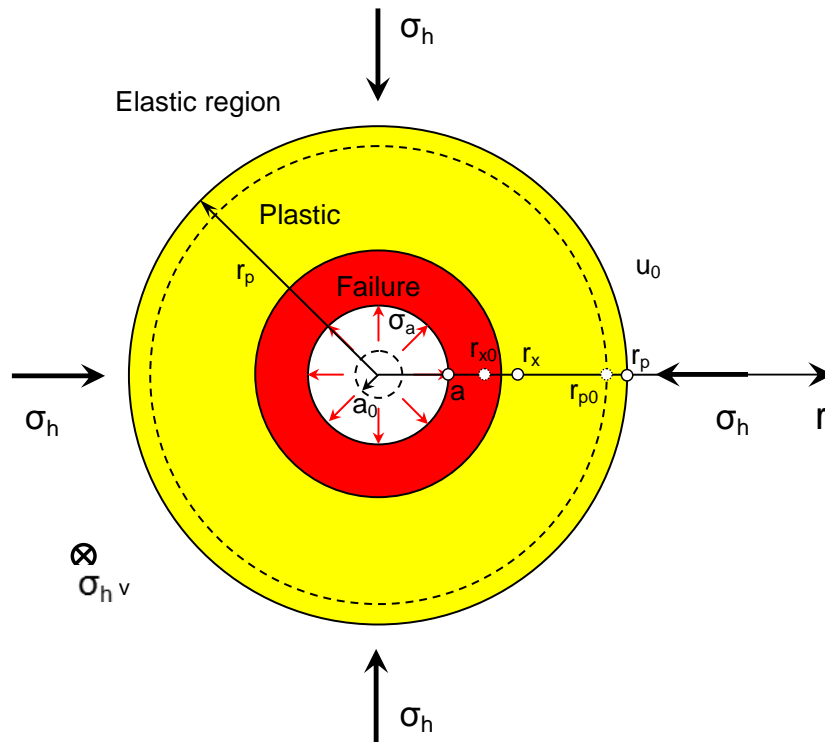


Fig. 4. Schematic of cavity expansion in anisotropic Cam Clay soil (Cylindrical) of a corresponding to the cavity pressure σ_a , and where plastic deformation is occurring throughout the annulus region $a \leq r \leq r_p$, in which r_p is the position of elastic-plastic boundary that is occupied by the material particle initial at r_{p0} (see Fig. 4). The symbol r_x refers to an

arbitrary point located in the plastic zone with its initial position denoted by r_{x0} . The soil beyond the plastic zone would remain in a state of elastic equilibrium.

Since the deformation mechanism of the soil around the shaft and tip of the piezocone are extremely similar to expansion of a spherical cavity and a cylindrical cavity, the measured readings from CPTu can be reasonably interpreted/analyzed based on spherical and/or cylindrical cavity expansion theories towards establishing a suite of soil parameters needed in analysis and design of construction projects.

1.3. Geological Environment

It is well known that soils in Southern Louisiana are characterized by soft consistency/low strength and high water content. Since the effect of the stress history and state dependent behaviours of clays can be reasonably by the Modified Cam Clay model, it is most appropriate to employ the Cam Clay critical state plasticity model for evaluating the soil properties from CPTu data, including the undrained shear strength s_u , overconsolidation ratio, and some other parameters. In this report, the modified Cam Clay model is adopted, the yield function of which can be expressed as follows

$$F(p', q, p'_c) = q^2 - M^2[p'(p'_c - p')] \quad (1.1)$$

in which p' and q , respectively, state the effective mean stress and deviatoric stress; p'_c is the yield pressure under isotropic compression, which, as the hardening parameter, essentially controls the size of current ellipsoidal yield locus; M specifies the slope of critical state line in $p' - q$ plane.

1.4. Important Statements

In this study, compressive stresses, strains and pore water pressure are taken conventionally as positive.

It is necessary to point out that the rigorous definitions for mean effective stress p' and deviatoric stress q are adopted in order to keep the rigor of analytical study. p' and q , respectively, take the following expressions

$$p' = \frac{\sigma'_r + \sigma'_\theta + \sigma'_z}{3} \quad (1.2)$$

$$q = \sqrt{\frac{1}{2}[(\sigma'_r - \sigma'_\theta)^2 + (\sigma'_\theta - \sigma'_z)^2 + (\sigma'_z - \sigma'_r)^2]} \quad (1.3)$$

in which σ'_r , σ'_θ and σ'_z represent the three effective principal stress components in the radial, tangential and vertical directions, respectively.

Compared with the existing studies (Carter et al., 1986; Cao et al., 2001) that assumed shear and Young's moduli G and E as constants during the analysis of cavity problem, this study will use their rigorous definitions, which, respectively, adopt

$$G = \frac{3(1-2\mu)vp'}{2(1+\mu)\kappa} \quad (1.4)$$

$$E = 2G(1 + \mu) \quad (1.5)$$

where μ specifies Poisson's ratio in drained; v is the specific volume; κ denotes the slope of swelling line in $v - \ln p'$ plane.

In addition, Mayne (1991) and Cao et al. (2001) showed that plastic volumetric strain ratio Λ , defined as $(\lambda - \kappa)/\lambda$, took the values of 0.75, 0.8 and 0.85 in the triaxial compression, simple shear, and triaxial extension tests, respectively. As Λ varies insignificantly, this report assumes that throughout the CPTu test Λ is a constant and is equal to 0.75.

1.5. Objective of Research

The main objective of this report is to analyze the penetration mechanism at both cone face and friction sleeve sections during CPTu test in modified Cam Clay soil, and to propose an exact interpretation method for the interpretation of the properties of soils from CPTu testing profiles. Specific objectives to accomplish the goal include:

(1) To present an exact semi-analytical solution for spherical cavity expansion in modified Cam Clay soil, which will serve as the theoretical basis for the modelling of the penetration mechanism at cone face section;

(2) To present an exact semi-analytical solution for cylindrical cavity expansion in modified Cam Clay soil, which will serve as the theoretical basis for the modelling of the penetration mechanism at friction sleeve section;

(3) To propose an exact interpretation model to explain the dependences of soil properties such as s_u , OCR, and $M [=6\sin\phi'/(3 - \sin\phi')]$ on the piezocone testing profiles, such as q_c , f_s , u_t , u_{bt} and u_{bs} ;

(4) To back calculate the properties of soil from CPTu testing profiles based on the proposed model.

1.6. Report Outline

This report has the following additional chapters:

Chapter 2 analyzes the mechanism of expanding a cylindrical cavity in undrained modified Cam Clay soils, and then presents relevant equations used to extract the properties of soil from CPTu testing profiles.

Chapter 3 analyzes the mechanism of expanding a spherical cavity in undrained modified Cam Clay soils, and then presents relevant equations used to extract the properties of soil from CPTu testing profiles.

Chapter 4 proposes an exact interpretation model used to extract the properties of soil from CPTu testing profiles, and focuses on the application of the proposed interpretation method.

Chapter 5 discusses the development of interpretation simulator, with which the back-calculation of the properties of soil becomes easier and convenient.

Chapter 6 consists of conclusions and recommendations for further research.

CHAPTER 2. ANALYSIS OF CPTU TEST USING SPHERICAL CAVITY THEORY

Teh and Housby (1991) showed that the penetration at cone face section can be modelled as the expansion of an existing spherical cavity to infinite. Hence, spherical cavity expansion theory is able to provide a theoretical framework for the penetration mechanism of cone face section.

On the basis of the above findings, this chapter mainly analyzes the elastoplastic response of soil around cone face during CPTu test, and discusses the corresponding penetration mechanism. At the end of this chapter, exact and explicit solutions for effective radial stress at failure state at cavity wall are developed, upon which an interpretation model used to back calculate the properties of soils is able to be proposed.

Note that in the spherical coordinate system the two tangential components θ and φ are the same due to the symmetry of the defined problem in this chapter (see Fig. 5).

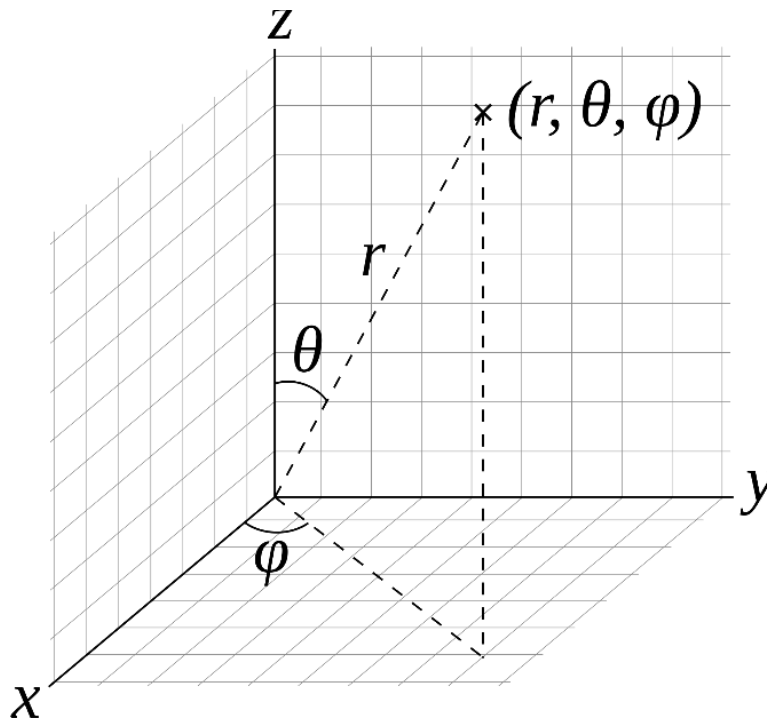


Fig. 5. Spherical Coordinate System

2.1. Elastic Analysis

Beyond elastic/plastic interface, soil remains in an elastic state and therefore needs to obey Hooke's law, by which stress-strain relationship can be expressed as

$$\begin{bmatrix} d\varepsilon_r \\ d\varepsilon_\theta \\ d\varepsilon_\varphi \end{bmatrix} = \frac{1}{E} \begin{bmatrix} 1 & -\mu & -\mu \\ -\mu & 1 & -\mu \\ -\mu & -\mu & 1 \end{bmatrix} \begin{bmatrix} d\sigma'_r \\ d\sigma'_\theta \\ d\sigma'_\varphi \end{bmatrix} \quad (2.1)$$

where $d\varepsilon_r$, $d\varepsilon_\theta$, $d\varepsilon_z$, and $d\sigma'_r$, $d\sigma'_\theta$, $d\sigma'_z$ are the three principal strain and stress increments, respectively, in radial, tangential and vertical directions.

According to elasticity (Yu, 2000; Timoshenko and Goodier, 1970), the distributions of stress components σ_r , σ_θ and σ_φ as well as radial displacement u_r can be expressed, in spherical coordinate system, as

$$\sigma_r = \sigma_h + (\sigma_p - \sigma_h) \left(\frac{r_p}{r}\right)^3 \quad (2.2.a)$$

$$\sigma_\theta = \sigma_h - \frac{1}{2}(\sigma_p - \sigma_h) \left(\frac{r_p}{r}\right)^3 \quad (2.2.b)$$

$$\sigma_\varphi = \sigma_\theta \quad (2.2.c)$$

$$u_r = \frac{\sigma_p - \sigma_h}{4G_0} \left(\frac{r_p}{r}\right)^3 r \quad (2.2.d)$$

in which σ_r and σ_θ represent the total radial and tangential stress components, respectively; σ_p is the total radial stress acting on the elastic/plastic interface r_p ; r specifies the position of the analyzed soil element; G_0 is the initial value of shear modulus G .

The analysis of spherical expansion of cavity is conducted in undrained condition, which requires that no volume change allows to occur throughout the expansion (Chen and Abousleiman, 2012). On the other hand, the volumetric strain increment $d\varepsilon_v$ can be calculated from Eq. (2.1)

as

$$d\varepsilon_v = d\varepsilon_r + d\varepsilon_\theta + d\varepsilon_\varphi = \frac{3(1-2\mu)}{E} dp' = 0 \quad (2.3)$$

To satisfy Eq. (2.3), mean effective stress p' has to maintain unchanged and is equal to the initial mean effective stress p'_0 (Chen and Abousleiman, 2012; Zhang et al., 2016).

$$p' = p'_0 \quad (2.4)$$

By adding equations (2.2.a)-(2.2.c), it is found that for any particle in external elastic region there is no variation in the total mean stress p , and consequently no excess pore pressure Δu is induced, because as noted above effective mean stress p' is also constant during elastic region (Chen and Abousleiman, 2012). Therefore,

$$u = u_0 \quad (2.5)$$

In addition, based on the definitions for shear and Young's moduli G and E (Eqs. (1.4)-(1.5)), it requires that these two parameters also have to hold constant during the elastic expansion of spherical cavity because of $p' = p'_0$ as given in Eq. (2.4), and are equal in magnitude to their own initial values at in-situ state of stresses (Chen and Abousleiman, 2012).

$$G = G_0 \quad (2.6.a)$$

$$E = E_0 \quad (2.6.b)$$

in which E_0 is the initial value of E .

2.2. Elastoplastic Analysis

With further expansion, soil around cavity wall behaves in an elastoplastic manner. Considering the symmetry of the defined spherical problem $\theta = \varphi$, total strains in the radial and tangential directions, respectively, can be written as

$$d\varepsilon_r = d\varepsilon_r^e + d\varepsilon_r^p \quad (2.7.a)$$

$$d\varepsilon_\theta = d\varepsilon_\theta^e + d\varepsilon_\theta^p \quad (2.7.b)$$

in which Hooke's Law defines the elastic strain increments $d\varepsilon_r^e$ and $d\varepsilon_\theta^e$; $d\varepsilon_r^p$ and $d\varepsilon_\theta^p$, which will be calculated in the following sections, specify the plastic strain increments in the radial and tangential directions.

To determined $d\varepsilon_r^p$ and $d\varepsilon_\theta^p$, the associated flow rule is assumed with modified Cam Clay model by means of normality condition. Therefore, one has

$$d\varepsilon_r^p = \Pi \frac{\partial F}{\partial \sigma_r'} = \Pi \left(\frac{\partial F}{\partial p'} \frac{\partial p'}{\partial \sigma_r'} + \frac{\partial F}{\partial q} \frac{\partial q}{\partial \sigma_r'} \right) = \Pi \left[\frac{(M^2 - \eta^2)p'}{3} + 3(\sigma_r' - p') \right] \quad (2.8.a)$$

$$d\varepsilon_\theta^p = \Pi \frac{\partial F}{\partial \sigma_\theta'} = \Pi \left(\frac{\partial F}{\partial p'} \frac{\partial p'}{\partial \sigma_\theta'} + \frac{\partial F}{\partial q} \frac{\partial q}{\partial \sigma_\theta'} \right) = \Pi \left[\frac{(M^2 - \eta^2)p'}{3} + 3(\sigma_\theta' - p') \right] \quad (2.8.b)$$

where Π is a scalar multiplier, also known as loading index; η , defined as $\eta = \frac{q}{p'}$, represents stress ratio.

On the basis of modified Cam Clay model, Wood (1990) obtained the plastic volumetric strain increment $d\varepsilon_p^p$, which reads

$$d\varepsilon_p^p = \frac{\lambda - \kappa}{vp'^2(M^2 + \eta^2)} \left\{ [p'(M^2 - \eta^2)] dp' + \frac{2\eta}{M^2 - \eta^2} [p'(M^2 - \eta^2)] dq \right\} \quad (2.9)$$

in which λ is the slope of compression line in $v - \ln p'$ plane.

On the other hand, plastic volumetric strain increment $d\varepsilon_p^p$ is equal to the sum of the three principal strain increments. Thus, it has

$$d\varepsilon_p^p = d\varepsilon_r^p + 2d\varepsilon_\theta^p \quad (2.10)$$

Substituting Eqs. (2.8.a)-(2.8.b) into Eq. (2.10) and taking into account the expression of $d\varepsilon_p^p$ in Eq. (2.9), the scalar multiplier Π can be finally determined as

$$\Pi = \frac{\lambda - \kappa}{\nu p'^2 (M^2 + \eta^2)} \left[dp' + \frac{2\eta}{M^2 - \eta^2} dq \right] \quad (2.11)$$

Therefore, the radial and tangential plastic strain increments $d\varepsilon_r^p$ and $d\varepsilon_\theta^p$ can be eventually rewritten as

$$d\varepsilon_r^p = \frac{\lambda - \kappa}{\nu p'^2 (M^2 + \eta^2)} \cdot \left[dp' + \frac{2\eta}{M^2 - \eta^2} dq \right] \cdot \left[\frac{M^2 - \eta^2}{3} p' + 3(\sigma_r' - p') \right] \quad (2.12.a)$$

$$d\varepsilon_\theta^p = \frac{\lambda - \kappa}{\nu p'^2 (M^2 + \eta^2)} \cdot \left[dp' + \frac{2\eta}{M^2 - \eta^2} dq \right] \cdot \left[\frac{M^2 - \eta^2}{3} p' + 3(\sigma_\theta' - p') \right] \quad (2.12.b)$$

Note that the rigorous definitions for mean effective stress p' and deviatoric stress q in Eqs. (1.2)-(1.3) are assumed throughout the analysis in this paper, and their incremental forms in spherical coordinate system should take the following relationships

$$dp' = \frac{d\sigma_r' + 2d\sigma_\theta'}{3} \quad (2.13.a)$$

$$dq = \frac{3(\sigma_r' - p')}{2q} d\sigma_r' + \frac{3(\sigma_\theta' - p')}{q} d\sigma_\theta' \quad (2.13.b)$$

Combining Eqs. (2.12)-(2.13), the radial and tangential plastic strain increments $d\varepsilon_r^p$ and $d\varepsilon_\theta^p$ also read

$$d\varepsilon_r^p = y \cdot \left\{ \left[\frac{p'(M^2 - \eta^2)}{3} + 3(\sigma_r' - p') \right] d\sigma_r' + \left[\frac{2p'(M^2 - \eta^2)}{3} + 6(\sigma_r' - p') \right] d\sigma_\theta' \right\} \cdot \left[\frac{M^2 - \eta^2}{3} p' + 3(\sigma_r' - p') \right] \quad (2.14.a)$$

$$d\varepsilon_\theta^p = y \cdot \left\{ \left[\frac{p'(M^2 - \eta^2)}{3} + 3(\sigma_r' - p') \right] d\sigma_r' + \left[\frac{2p'(M^2 - \eta^2)}{3} + 6(\sigma_\theta' - p') \right] d\sigma_\theta' \right\} \cdot \left[\frac{M^2 - \eta^2}{3} p' + 3(\sigma_\theta' - p') \right] \quad (2.14.b)$$

where

$$y = \frac{\lambda - \kappa}{vp'^3(M^4 - \eta^4)} \quad (2.14.c)$$

Assuming the following relationships

$$a_r = \frac{p'(M^2 - \eta^2)}{3} + 3(\sigma'_r - p') \quad (2.14.d)$$

$$a_\theta = \frac{p'(M^2 - \eta^2)}{3} + 3(\sigma'_\theta - p') \quad (2.14.e)$$

Eqs. (2.14.a)-(2.14.b) can be rewritten in a simple way as

$$d\varepsilon_r^p = y \cdot \{a_r d\sigma'_r + 2a_\theta d\sigma'_\theta\} \cdot a_r \quad (2.15.a)$$

$$d\varepsilon_\theta^p = y \cdot \{a_r d\sigma'_r + 2a_\theta d\sigma'_\theta\} \cdot a_\theta \quad (2.15.b)$$

or

$$\begin{Bmatrix} d\varepsilon_r^p \\ d\varepsilon_\theta^p \end{Bmatrix} = y \begin{bmatrix} a_r^2 & 2a_r a_\theta \\ a_r a_\theta & 2a_\theta^2 \end{bmatrix} \begin{Bmatrix} d\sigma'_r \\ d\sigma'_\theta \end{Bmatrix} \quad (2.16)$$

Taking into account the recoverable strains during elastoplastic deformation

$$\begin{Bmatrix} d\varepsilon_r \\ d\varepsilon_\theta \end{Bmatrix} = \begin{bmatrix} \frac{1}{E} + ya_r^2 & -\frac{2\mu}{E} + 2ya_r a_\theta \\ -\frac{\mu}{E} + ya_r a_\theta & \frac{1-\mu}{E} + 2ya_\theta^2 \end{bmatrix} \begin{Bmatrix} d\sigma'_r \\ d\sigma'_\theta \end{Bmatrix} \quad (2.17)$$

Inverse of the matrix in Eq. (2.17) gives

$$\begin{Bmatrix} d\sigma'_r \\ d\sigma'_\theta \end{Bmatrix} = \frac{1}{\Delta} \begin{bmatrix} b_{11} & b_{12} \\ b_{21} & b_{22} \end{bmatrix} \begin{Bmatrix} d\varepsilon_r \\ d\varepsilon_\theta \end{Bmatrix} \quad (2.18.a)$$

in which

$$b_{11} = E(1 - \mu + 2a_\theta^2 y E) \quad (2.18.b)$$

$$b_{12} = 2E(\mu - a_r a_\theta y E) \quad (2.18.c)$$

$$b_{21} = E(\mu - a_r a_\theta \gamma E) \quad (2.18.d)$$

$$b_{22} = E(1 + a_r^2 \gamma E) \quad (2.18.e)$$

$$\Delta = 1 - 2\mu^2 + a_r^2 \gamma E + 2a_\theta^2 \gamma E - \mu(1 + a_r^2 \gamma E - 4a_r a_\theta \gamma E) \quad (2.18.f)$$

To consider the effect of large deformation in plastic region, logarithmic strain definitions are adopted, which take the following relationships

$$d\varepsilon_r = -\frac{\partial(dr)}{\partial r} \quad (2.19.a)$$

$$d\varepsilon_\theta = -\frac{dr}{r} \quad (2.19.b)$$

Considering the volume conservation in undrained condition and then substituting Eqs. (2.19) into Eq. (2.18.a), the solutions in plastic region are finally reduced to solving the following partial differential equations

$$\frac{D\sigma'_r}{Dr} = \frac{2b_{11}-b_{12}}{\Delta r} \quad (2.20.a)$$

$$\frac{D\sigma'_\theta}{Dr} = \frac{2b_{21}-b_{22}}{\Delta r} \quad (2.20.b)$$

where D/Dr denotes the material derivative taken along the particle motion path. Eqs. (2.20) are valid for any material point r_x currently located in the plastic zone, and contain two unknown stress σ'_r and σ'_θ as functions of a single variable r , which varies from r_{xp} to r_x . Here r_{xp} represents the position of the specific particle when it is just entering into the plastic state. To solve these partial differential equations one needs a prior knowledge of r_{xp} as well as the corresponding initial values $\sigma'_r(\sigma'_{xp})$ and $\sigma'_\theta(\sigma'_{xp})$.

2.3. Boundary Value Problem

From the yield function of modified Cam Clay model in Eq. (1.1), the preconsolidation pressure p_c , the mean effective stress p'_p and deviatoric stress q_p at the elastic/plastic boundary are calculated as

$$p_c = Rp_A = R\left(\frac{q_0^2}{M^2 p_0} + p_0\right) \quad (2.21.a)$$

$$p'_p = p'_0 \quad (2.21.b)$$

$$q_p = Mp'_0 \sqrt{R\left(\frac{1}{M^2} \frac{q_0^2}{p_0'^2} + 1\right) - 1} \quad (2.21.c)$$

Furthermore, soil elements at the elastic/plastic interface have to satisfy both the elastic and elastoplastic requirements. Therefore, the stress components (Cao et al., 2001; Chang et al., 2001) at the elastic/plastic interface as well as the radial position of the elastic/plastic interface can be determined as

$$\sigma'_{rp} = p'_0 + \frac{2}{3}q_p \quad (2.21.d)$$

$$\sigma'_{\theta p} = p'_0 - \frac{1}{3}q_p \quad (2.21.e)$$

$$\frac{r_{xp}}{a} = \frac{1}{1 - \frac{\sigma'_{rp} - \sigma'_{r0}}{4G_0}} \sqrt[3]{\left(\frac{r_x}{a}\right)^3 + \left(\frac{a_0}{a}\right)^3 - 1} \quad (2.21.f)$$

$$\frac{r_p}{a} = \sqrt[3]{\frac{\left(\frac{a_0}{a}\right)^3 - 1}{\left(1 - \frac{\sigma'_{rp} - \sigma'_{r0}}{4G_0}\right)^3 - 1}} \quad (2.21.g)$$

2.4. Stress Components at Failure State

Sections 2.1-2.3 analyze the undrained expansion of a spherical cavity in modified Cam Clay soil and correspondingly present an exact semi-analytical solution. However, the presented semi-analytical solution cannot be directly used for the interpretation of the properties of soil from CPTu testing profiles at cone face, due to the inability of Mathematica to solve the partial differential equations. To overcome the above difficulties, this section aims to find a set of exact but explicit expressions of soil properties.

Undrained condition restrains the volume of soil from changing during cavity expansion. Thus, it requires

$$d\varepsilon_p^e + d\varepsilon_p^p = 0 \quad (2.22.a)$$

where

$$d\varepsilon_p^e = \kappa \frac{dp'}{vp'} \quad (2.22.b)$$

$$d\varepsilon_p^p = (\lambda - \kappa) \frac{dp'_c}{vp'_c} \quad (2.22.c)$$

Substituting Eqs. (2.22.b)-(2.22.c) into Eq. (2.22.a), it has

$$\kappa \frac{dp'}{vp'} = -(\lambda - \kappa) \frac{dp'_c}{vp'_c} \quad (2.22.d)$$

Taking the integral of left hand side and right hand side of Eq. (2.22.d) over the intervals $[p'_0, p']$ and $[p'_{c0}, p'_c]$, respectively, it has

$$\left(\frac{p'}{p'_0}\right)^{(-\frac{1}{\lambda}+1)} = \frac{p'_c}{p'_{c0}} \quad (2.23)$$

Substituting the yield function of modified Cam Clay model in Eq. (1.1) into Eq. (2.23), the following relationship can be obtained (Cao et al., 2001)

$$\frac{q^2}{M^2 p'} + p' = p'_{c0} \left(\frac{p'}{p_0}\right)^{\left(-\frac{1}{\lambda}+1\right)} \quad (2.24)$$

Assuming $p'_{c0} = R \cdot p'_0$, the above equation can be further simplified as

$$q = Mp' \sqrt{R \left(\frac{p'}{p_0}\right)^{-\frac{1}{\lambda}} - 1} \quad (2.25)$$

The symmetry of spherical cavity expansion $\theta = \varphi$ allows q to be written as

$$q = \sigma'_r - \sigma'_\theta \quad (2.26)$$

Combining the two equations (2.25)-(2.26), the exact but explicit expressions of effective radial and tangential stresses σ'_r and σ'_θ can be expressed, respectively, as

$$\sigma'_r = p' + \frac{2}{3} Mp' \sqrt{R \left(\frac{p'}{p_0}\right)^{-\frac{1}{\lambda}} - 1} \quad (2.27.a)$$

$$\sigma'_\theta = p' - \frac{1}{3} Mp' \sqrt{R \left(\frac{p'}{p_0}\right)^{-\frac{1}{\lambda}} - 1} \quad (2.27.b)$$

At failure state, Cao et al. (2001) derived the ultimate mean effective stress p'_u and ultimate deviatoric stress q_u as given by

$$q_u = Mp'_u \quad (2.28.a)$$

$$p'_u = p'_0 \left(\frac{R}{2}\right)^\lambda \quad (2.28.b)$$

$$q_u = Mp'_u = Mp'_0 \left(\frac{R}{2}\right)^\lambda \quad (2.28.c)$$

Hence, the stress components $\sigma'_{r,u}$ and $\sigma'_{\theta,u}$ at failure state are able to be obtained and given by the following relationships

$$\sigma'_{r,u} = p'_u + \frac{2}{3} Mp'_u \quad (2.29.a)$$

$$\sigma'_{\theta,u} = p'_u - \frac{1}{3}Mp'_u \quad (2.29.b)$$

2.5. Summary

Based on spherical cavity theory and modified Cam Clay model, this chapter presents an exact semi-analytical solution for the elastoplastic response of soil around cone face during CPTu test, and proposes an exact but explicit interpretation method for the determination of the properties of soil from CPTu testing at cone face.

In this chapter, an exact semi-analytical solution for spherical cavity expansion in modified Cam Clay soil is firstly presented. It is found that the defined problem can be finally reduced to solving two partial differential equations, with stress components being the basic unknowns. However, the properties of soil cannot be back calculated directly by solving these two equations because of the inability of Mathematica.

At the end of this chapter, exact expressions are developed that have the potential to explicitly express the properties of soil. Taking advantage of undrained condition, effective stress path of a given soil element in $p' - q$ plane is able to be determined. Thereafter, the symmetry of the defined problem makes possible the explicit expressions of stress components for any soil element.

CHAPTER 3. ANALYSIS OF CPTU TEST USING CYLINDRICAL CAVITY THEORY

Teh and Houlsby (1991) has shown that the penetration at the friction sleeve could be considered as the process of expanding an existing cylindrical cavity to infinite. Based on this fact, this chapter mainly discusses during CPTu test the response of soil around friction sleeve and analyzes the corresponding penetration mechanism. Exact but explicit solutions for the ultimate stress components at cavity wall are developed, which may be further extended for the interpretation of the properties of soil from CPTu profiles.

3.1. Elastic Analysis

The stress strain relationship in cylindrical coordinate system can be written as

$$\begin{bmatrix} d\varepsilon_r \\ d\varepsilon_\theta \\ d\varepsilon_z \end{bmatrix} = \frac{1}{E} \begin{bmatrix} 1 & -\mu & -\mu \\ -\mu & 1 & -\mu \\ -\mu & -\mu & 1 \end{bmatrix} \begin{bmatrix} d\sigma'_r \\ d\sigma'_\theta \\ d\sigma'_z \end{bmatrix} \quad (3.1)$$

where $d\varepsilon_z$ and $d\sigma'_z$, respectively, specify the strain and effective stress increments in vertical direction.

Yu (2000) obtained the distributions of σ_r , σ_θ and σ_z as well as u_r , which, respectively ,read

$$\sigma_r = \sigma_h + (\sigma_p - \sigma_h) \left(\frac{r_p}{r}\right)^2 \quad (3.2.a)$$

$$\sigma_\theta = \sigma_h - (\sigma_p - \sigma_h) \left(\frac{r_p}{r}\right)^2 \quad (3.2.b)$$

$$\sigma_z = \sigma_v \quad (3.2.c)$$

$$u_r = \frac{\sigma_p - \sigma_h}{2G_0} \left(\frac{r_p}{r}\right)^2 r \quad (3.2.d)$$

in which σ_z represents the total vertical stress.

Chen and Abousleiman (2012) demonstrated that in cylindrical coordinate system mean effective stress p' still held constant, and was equal to its initial value of p'_0 .

$$d\varepsilon_v = d\varepsilon_r + d\varepsilon_\theta + d\varepsilon_z = \frac{3(1-2\mu)}{E} dp' = 0 \quad (3.3)$$

$$p' = p'_0 \quad (3.4)$$

Correspondingly, it is also found that pore water pressure u maintained unchanged (Chen and Abousleiman, 2012).

$$u = u_0 \quad (3.5)$$

Hence, shear and Young's moduli G and E in elastic region are able to be determined as

$$G = G_0 \quad (3.6.a)$$

$$E = E_0 \quad (3.6.b)$$

3.2. Elastoplastic Analysis

Chen and Abousleiman (2012) presented an exact semi-analytical solution for cylindrical cavity expansion in modified Cam Clay critical state soil under the undrained condition. To avoid the lengthiness of the report, please refer to this paper for the details.

The plastic flow rule is taken to be associated, resulting in the plastic strain increments being

$$d\varepsilon_r^p = \Pi \frac{\partial F}{\partial \sigma'_r} = \Pi \left[\frac{p'(M^2 - \eta^2)}{3} + 3(\sigma'_r - p') \right] \quad (3.7.a)$$

$$d\varepsilon_\theta^p = \Pi \frac{\partial F}{\partial \sigma'_\theta} = \Pi \left[\frac{p'(M^2 - \eta^2)}{3} + 3(\sigma'_\theta - p') \right] \quad (3.7.b)$$

$$d\varepsilon_z^p = \Pi \frac{\partial F}{\partial \sigma'_z} = \Pi \left[\frac{p'(M^2 - \eta^2)}{3} + 3(\sigma'_z - p') \right] \quad (3.7.c)$$

where $d\varepsilon_z^p$ is the plastic strain increment in vertical direction.

Following the same procedures, the scalar multiplier Π in the cylindrical condition can be determined as

$$\Pi = \frac{\lambda - \kappa}{vp'^2(M^2 + \eta^2)} (dp' + \frac{2\eta}{M^2 - \eta^2} dq) \quad (3.8)$$

It gives the following relationship by substituting Eq. (3.8) into Eqs. (3.7)

$$\begin{Bmatrix} d\varepsilon_r^p \\ d\varepsilon_\theta^p \\ d\varepsilon_z^p \end{Bmatrix} = y \begin{bmatrix} a_r^2 & a_r a_\theta & a_r a_z \\ a_\theta a_r & a_\theta^2 & a_\theta a_z \\ a_z a_r & a_z a_\theta & a_z^2 \end{bmatrix} \begin{Bmatrix} d\sigma_r' \\ d\sigma_\theta' \\ d\sigma_z' \end{Bmatrix} \quad (3.9.a)$$

where

$$y = \frac{\lambda - \kappa}{vp'^3(M^4 - \eta^4)} \quad (3.9.b)$$

$$a_r = \frac{p'(M^2 - \eta^2)}{3} + 3(\sigma_r' - p') \quad (3.9.c)$$

$$a_\theta = \frac{p'(M^2 - \eta^2)}{3} + 3(\sigma_\theta' - p') \quad (3.9.d)$$

$$a_z = \frac{p'(M^2 - \eta^2)}{3} + 3(\sigma_z' - p') \quad (3.9.e)$$

Taking into account the elastic recoverable strains, it has

$$\begin{Bmatrix} d\varepsilon_r^p \\ d\varepsilon_\theta^p \\ d\varepsilon_z^p \end{Bmatrix} = \begin{bmatrix} \frac{1}{E} + ya_r^2 & -\frac{\mu}{E} + ya_r a_\theta & -\frac{\mu}{E} + ya_r a_z \\ -\frac{\mu}{E} + ya_\theta a_r & \frac{1}{E} + ya_\theta^2 & -\frac{\mu}{E} + ya_\theta a_z \\ -\frac{\mu}{E} + ya_z a_r & -\frac{\mu}{E} + ya_z a_\theta & \frac{1}{E} + ya_z^2 \end{bmatrix} \begin{Bmatrix} d\sigma_r' \\ d\sigma_\theta' \\ d\sigma_z' \end{Bmatrix} \quad (3.10)$$

Inverse of the matrix in Eq. (3.10) gives

$$\begin{Bmatrix} d\sigma'_r \\ d\sigma'_\theta \\ d\sigma'_z \end{Bmatrix} = \frac{1}{\Delta} \begin{bmatrix} b_{11} & b_{12} & b_{13} \\ b_{21} & b_{22} & b_{23} \\ b_{31} & b_{32} & b_{33} \end{bmatrix} \begin{Bmatrix} d\varepsilon_r^p \\ d\varepsilon_\theta^p \\ d\varepsilon_z^p \end{Bmatrix} \quad (3.11.a)$$

in which

$$b_{11} = \frac{1}{E^2} (1 - \mu^2 + Ea_\theta^2 y + 2E\mu a_\theta a_z y + Ea_z^2 y) \quad (3.11.b)$$

$$b_{12} = \frac{1}{E^2} [-Ea_r(a_\theta + \mu a_z)y + \mu(1 + \mu - Eya_\theta a_z + Ea_z^2 y)] \quad (3.11.c)$$

$$b_{13} = \frac{1}{E^2} [-Ea_r(\mu a_\theta + a_z)y + \mu(1 + \mu + Eya_\theta^2 - Eya_\theta a_z)] \quad (3.11.d)$$

$$b_{22} = \frac{1}{E^2} [1 - \mu^2 + Eya_r^2 + 2E\mu ya_r a_z + Eya_z^2] \quad (3.11.e)$$

$$b_{23} = \frac{1}{E^2} [\mu + \mu^2 + E\mu ya_r^2 - Eya_\theta a_z - E\mu a_r(a_z + a_\theta)y] \quad (3.11.f)$$

$$b_{33} = \frac{1}{E^2} [1 - \mu^2 + Eya_r^2 + 2E\mu ya_r a_\theta + Eya_\theta^2] \quad (3.11.g)$$

$$b_{21} = b_{12} \quad (3.11.h)$$

$$b_{31} = b_{13} \quad (3.11.i)$$

$$b_{32} = b_{23} \quad (3.11.j)$$

$$\Delta = -\frac{1+\mu}{E^3} [(-1 + \mu + 2\mu^2) + E(-1 + \mu)ya_r^2 + E(-1 + \mu)ya_\theta^2 - 2E\mu a_\theta a_z y - Eya_z^2 + E\mu ya_z^2 - 2E\mu a_r(a_z + a_\theta)y] \quad (3.11.k)$$

Large deformation effect is taken into account by adopting Eqs. (2.21). Combining Eqs. (2.21) and Eq. (3.11.a), the elastoplastic solutions are eventually reduced to the following three partial differential equations

$$\frac{D\sigma'_r}{Dr} = \frac{b_{11}-b_{12}}{\Delta r} \quad (3.12.a)$$

$$\frac{D\sigma'_\theta}{Dr} = \frac{b_{21}-b_{22}}{\Delta r} \quad (3.12.b)$$

$$\frac{D\sigma'_z}{Dr} = \frac{b_{31}-b_{32}}{\Delta r} \quad (3.12.c)$$

To solve the three partial differential equations as denoted in Eqs. (3.12.a)-(3.12.c), the initial boundary values has to be known as a priori, which will be discussed in the next section.

3.3. Boundary Value Problem

Soil element at elastic/plastic interface needs to satisfy both the elastic and plastic requirements. Therefore, the following initial values can be determined as

$$\sigma'_{rp} = \sigma'_{r0} + \sqrt{\sigma'_{r0}{}^2 - \frac{1}{3}(4\sigma'_{r0}{}^2 + \sigma'_{z0}{}^2 - 2\sigma'_{r0}\sigma'_{z0} - q_p^2)} \quad (3.13.a)$$

$$\sigma'_{\theta p} = \sigma'_{r0} - \sqrt{\sigma'_{r0}{}^2 - \frac{1}{3}(4\sigma'_{r0}{}^2 + \sigma'_{z0}{}^2 - 2\sigma'_{r0}\sigma'_{z0} - q_p^2)} \quad (3.13.b)$$

$$\sigma'_{zp} = \sigma'_{z0} = \frac{3}{1+2K_0} p'_0 \quad (3.13.c)$$

$$\frac{r_{xp}}{a} = \frac{1}{1 - \frac{\sigma'_{rp} - \sigma'_{r0}}{2G_0}} \sqrt{\left(\frac{r_x}{a}\right)^2 + \left(\frac{a_0}{a}\right)^2 - 1} \quad (3.13.d)$$

$$\frac{r_p}{a} = \sqrt{\frac{\left(\frac{a_0}{a}\right)^2 - 1}{\left(\frac{\sigma'_{rp} - \sigma'_{r0}}{2G_0}\right)^2 - \frac{\sigma'_{rp} - \sigma'_{r0}}{2G_0}}} \quad (3.13.e)$$

3.4. Stress Components at Failure State

After obtaining the above exact semi-analytical solutions, Chen and Abousleiman (2012) proposed the following equation in an attempt to analyze the relationship between the three principal stress components σ'_r , σ'_θ and σ'_z in the critical state region.

$$\frac{D}{Dr} (\sigma'_r + \sigma'_\theta - 2\sigma'_z) = - \frac{3(1-2\nu)(a_r - a_\theta)(\sigma'_r + \sigma'_\theta - 2\sigma'_z)y}{\Delta r E} \quad (3.14)$$

Eq. (3.14) indicates that the ultimate vertical effective stress $\sigma'_{z,u}$ has to satisfy the following relationship with $\sigma'_{r,u}$ and $\sigma'_{\theta,u}$

$$\sigma'_{z,u} = \frac{\sigma'_{r,u} + \sigma'_{\theta,u}}{2} \quad (3.15)$$

Combining Eqs. (1.2)-(1.3), Eqs. (2.28) and (3.15), the ultimate effective stress components, $\sigma'_{r,u}$, $\sigma'_{\theta,u}$ and $\sigma'_{z,u}$, can be explicitly determined as

$$\sigma'_{r,u} = p'_u + \frac{q_u}{\sqrt{3}} \quad (3.16.a)$$

$$\sigma'_{\theta,u} = p'_u - \frac{q_u}{\sqrt{3}} \quad (3.16.b)$$

$$\sigma'_{z,u} = p'_u \quad (3.16.c)$$

3.5. Summary

Based on cylindrical cavity theory and modified Cam Clay model, this chapter presents an exact semi-analytical solution for the elastoplastic response of soils around friction sleeve during CPTu test, and proposes an exact but explicit interpretation method for the determination of the properties of soil from CPTu testing at friction sleeve section.

This chapter begins with presenting an exact semi-analytical solution for undrained cylindrical cavity expansion in modified Cam Clay soil. It is found that the defined problem can be finally reduced to solving three partial differential equations, with stress components being the basic unknowns. However, the properties of soil cannot be back calculated directly by solving these three partial differential equations because of the limited calculation capabilities of Mathematica.

At the end of this chapter, exact expressions are developed that have the potential to explicitly express the properties of soil. On the basis of the exact semi-analytical solution for

cylindrical cavity expansion in undrained modified Cam Clay soil, it is found that in the failure state, vertical effective stress should always be equal in value to the mean of the effective radial and tangential stresses. Then a set of exact but explicit expressions of stress components at failure state are developed, and thereafter makes possible the interpretation of the properties of soil in an exact manner.

CHAPTER 4. INTERPRETATION OF CPTU TEST

This chapter proposes an exact interpretation method for the determination of the properties of soil from CPTu testing profiles based on the analysis in Chapter 2 and 3. As illustrative examples, two CPTu testing profiles at Brent and Grangemouth are subsequently analyzed and interpreted using this interpretation method.

Different from most of existing studies that only take into account the spherical cavity theory when interpreting CPTu test, this report attempts to simultaneously combine both the spherical and cylindrical cavity theories in the interpretation of the CPTu measurements. To achieve this purpose, three filters are placed purposely to measure the generated pore water pressure u_t , u_{bt} and u_{bs} , respectively, during the test. The schematic illustration of this basic configuration of CPTu device is shown in Fig. 6. Besides the three pore water pressure measurements, cone tip resistance and sleeve friction are the additional two measurements.

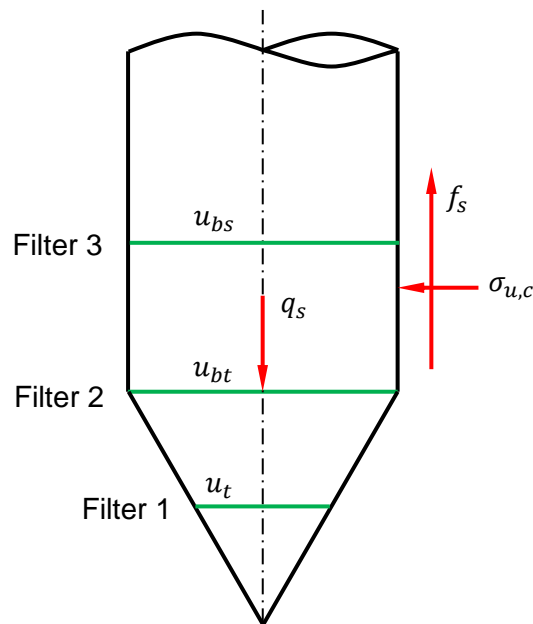


Fig. 6. Schematic illustration of CPTu device

4.1. CPTu Test and Measurement Corrections

CPTu test has been considered as an important tool for obtaining soil properties since its development in the early 1970s. It has the following advantages (Chen, B.S., 1994)

1. Testing under the in-situ ambient stress state;
2. Reduced sampling disturbance;
3. Continuous profiling;
4. Fast operation;
5. Relative low cost.

However, compared with other in-situ tests, CPTu requires a higher level of field and theoretical expertise to conduct and interpret. In the test, the correction of measurements is one of the procedures that need great attention.

4.1.1. Correction of Cone Tip Resistance q_c (Chen B.S., 1994)

Campanella et al. (1982) indicated the need for a correction of q_c for the pore pressures acting on the unequal end area behind the cone tip. This important correction was later supported by many other researchers (Lacasse and Lunne, 1982; Jamiolkowski et al., 1985; Battaglio et al. 1986; Lunne et al., 1986; Powell et al., 1988). Pore pressures generated during cone penetration act on the back of the cone tip as well as on the cone face (Fig. 7), resulting in a measured value of q_c that is less than the full magnitude of the total vertical resistance. The detailed mechanical condition of cone tip is schematically shown below in Fig. 8, from which the following equation regarding the vertical equilibrium condition can be constructed as

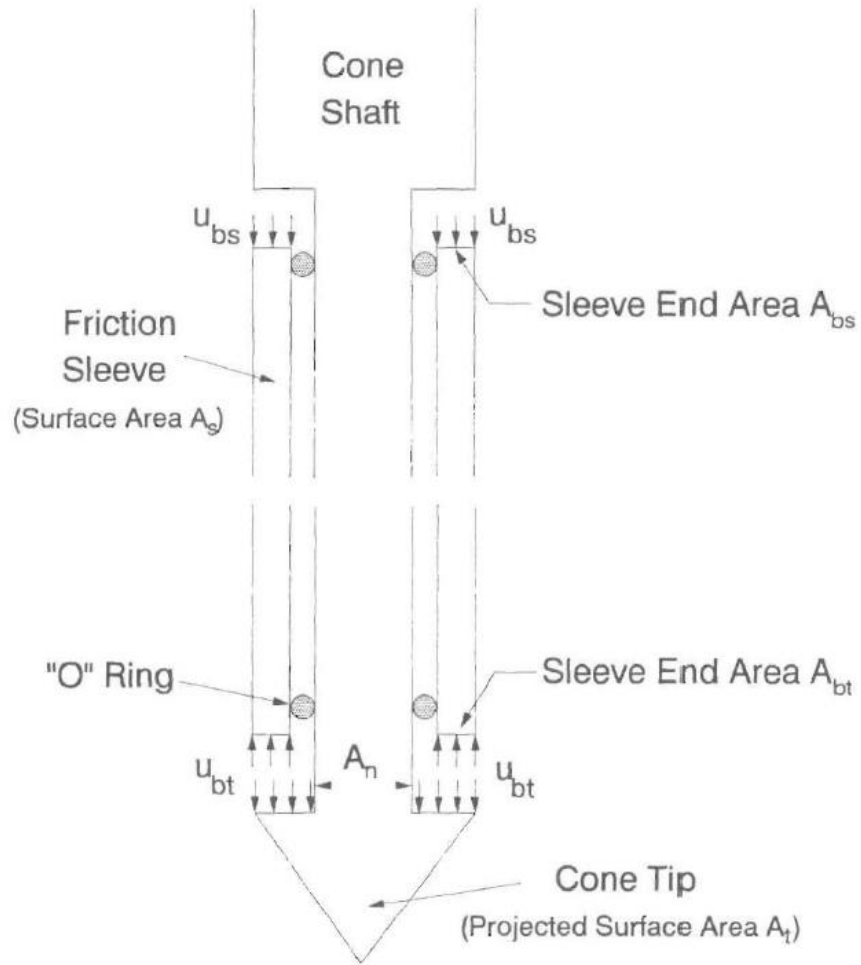


Fig. 7. Unequal end area of electric cone used for correcting q_c and f_s (after Chen B.S., 1994)

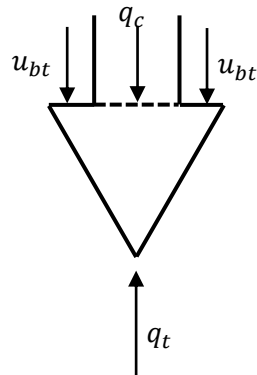


Fig. 8. Schematic illustration of mechanical equilibrium of cone face

$$q_t = q_c + (1 - \alpha)u_{bt} \tag{4.1}$$

where α is the effective area ratio, defined as $\alpha = \frac{A_n}{A_T}$ (see Fig. 5).

4.1.2. Correction of Sleeve Friction f_s (Chen B.S., 1994)

The measured sleeve friction also needs to be corrected to account for pore pressures acting on the unequal end areas of the upper (A_{bs}) and lower (A_{bt}) ends of the friction sleeve (Fig. 5). Based on the equilibrium condition of friction sleeve in vertical direction, it gives the following relationship

$$f_t = f_s + \frac{A_{bs}u_{bs} - A_{bt}u_{bt}}{A_s} \quad (4.2)$$

where u_{bs} and u_{bt} , respectively, specify the pore pressures measured behind the friction sleeve and the cone tip; A_s gives the surface area of friction sleeve. Here, it is necessary to point out that the correction is negligible, provided that same end areas are assumed on the sleeve (Chen B.S., 1994).

4.2. Interpretation Method

Teh and Houlsby (1991) showed that during CPTu test the penetration could be modelled as the expansion of an existing cavity to infinite. Therefore, for the penetration at cone face the ultimate radial effective stress $\sigma'_{a,s}$ is related to the measurements q_t and u_t by

$$\sigma'_{a,s} = q_t - u_t \quad (4.3)$$

Combining Eq. (4.3), Eq. (2.29.a) is rewritten as

$$q_t - u_t = p'_u + \frac{2}{3}Mp'_u \quad (4.4)$$

In addition, the ultimate effective cavity pressure $\sigma'_{a,c}$ acting on the friction sleeve can be linearly related by the coefficient of friction δ to the corrected friction f_t , as

$$\sigma'_{a,c} = \frac{f_t}{\delta} \quad (4.5)$$

in which Konrad and Law (1987) recommended that δ took the value of 0.5 to 0.75 for smooth steel and of 1.0 for normal roughness.

Considering the ultimate effective cavity pressure under cylindrical condition, respectively, in Eq. (3.16.a) and Eq. (4.5), it gives the following equation

$$\frac{f_t}{\delta} = p'_u + \frac{q_u}{\sqrt{3}} \quad (4.6)$$

4.2.1. Determination of Undrained Shear Strength $s_{u,s}$

The following relationship can be immediately obtained by combining Eq. (4.4) and Eq. (4.6).

$$(q_t - u_t) - \frac{f_t}{\delta} = \frac{2}{3} M p'_u - \frac{q_u}{\sqrt{3}} \quad (4.7)$$

Cao et al. (2001) developed the undrained shear strength $s_{u,s}$ and $s_{u,c}$, respectively, in spherical and cylindrical conditions, as

$$s_{u,s} = \frac{q_u}{2} \quad (4.8.a)$$

$$s_{u,c} = \frac{q_u}{\sqrt{3}} \quad (4.8.b)$$

With the aid of Eq. (4.8.a), Eq. (4.7) can be rewritten in terms of spherical undrained shear strength $s_{u,s}$ as

$$(q_t - u_t) - \frac{f_t}{\delta} = \frac{4}{3} s_{u,s} - \frac{2s_{u,s}}{\sqrt{3}} \quad (4.9)$$

Here, an empirical coefficient α_ε is introduced to account for the effects of strain rate during CPTu test on undrained shear strength. Note that since the cylindrical cavity expansion is

always after the spherical cavity expansion, hence there is no need to correct the cylindrical terms in Eq. (4.9). On the other hand, the undrained shear strength from the spherical cavity expansion should be corrected by α_ε . Based on Eq. (4.9), undrained shear strength $s_{u,s}$, thereafter, can be explicitly expressed as

$$s_{u,s} = \frac{(q_t - u_t) - \frac{f_s}{\delta}}{\frac{4}{3}\alpha_\varepsilon - \frac{2}{\sqrt{3}}} \quad (4.10)$$

4.2.2. Determination of Slope of Critical State Line M

Based on the definition for spherical undrained shear strength $s_{u,s}$, Eq. (4.4) can be rearranged in the form

$$q_t - u_t = \frac{2s_{u,s}}{M} + \frac{4}{3}s_{u,s} \quad (4.11)$$

from which, the slope of critical state line M in $p' - q$ plane can be explicitly expressed as

$$M = \frac{2}{\frac{q_t - u_t}{s_{u,s}} - \frac{4}{3}} \quad (4.12.a)$$

The corresponding effective internal friction angle ϕ' , by definition, can be determined by solving

$$M = 6 \sin \phi' / (3 - \sin \phi') \quad (4.12.b)$$

4.2.3. Determination of Overconsolidation Ratio OCR

The definition of undrained shear strength $s_{u,s}$ in spherical condition gives

$$s_{u,s} = \frac{q_u}{2} = \frac{1}{2} M p'_0 \left(\frac{OCR}{2} \right)^\Lambda \quad (4.13)$$

Hence, the explicit expression of overconsolidation ratio is presented in terms of M and $s_{u,s}$, as

$$OCR = 2\left(\frac{2s_{us}}{Mp_0'}\right)^{1/\Lambda} \quad (4.14)$$

4.3. Case Study

Two CPTu testing profiles at Brent and Grangemouth sites, respectively, are analyzed using the interpretation method proposed above.

4.3.1. CPTu Test at Brent

Geological records of prior soil borings indicated that the depth of 0 to 9 m was made of firm to stiff, very finely fissured sticky brown weathered London clay; Claystones were found at the depth of 12 to 13m; below 13m, stiff to very stiff highly fissured blue/grey unweathered London clay with thin layers of silt on some fissures was detected, along with occasional thin silty sand; fissure spacing was found to increase with depth. The density of the soils at testing site was around 1950 kg/m^3 .

For this test, a 10cm^2 cone was adopted with the penetration speed being 20mm/s. Powell et al. (1988) recommended the effective area ratio of $\alpha = 0.7\sim 0.8$ to correct the measured cone tip resistance q_c . In this case study, $\alpha = 0.75$ is used.

The obtained CPTu profile is shown in Fig. 9.

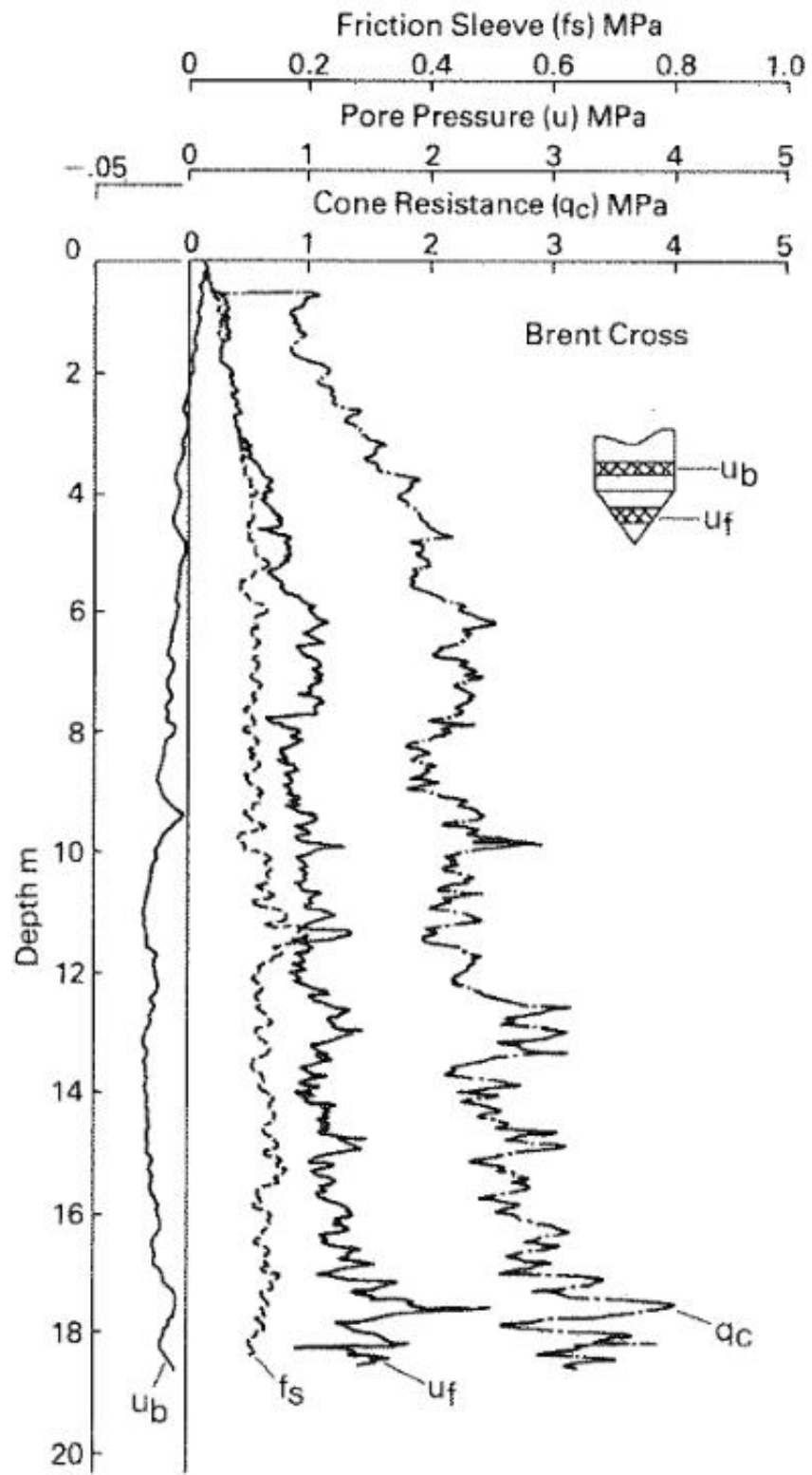


Fig.9. Typical Piezocone Profiles at Brent (after Powell et al., 1988)

Larsson and Mulabdic (1991) found that the pore water pressure on the cone shaft decreased with the increase of distance from the cone tip. Because CPTu test at Brent site adopted the cone with two filters – one was to monitor the pore water pressure u_t at cone tip, another one was to measure the pore water pressure u_{bt} behind the tip, thus u_{bt} is multiplied by a coefficient of 0.7 to assume the pore water pressure u_{bs} generated at the friction sleeve section.

Using the interpretation model elaborated in the previous section as well as the CPTu testing profiles in Fig. 10, the properties of soil at Brent are able to be determined.

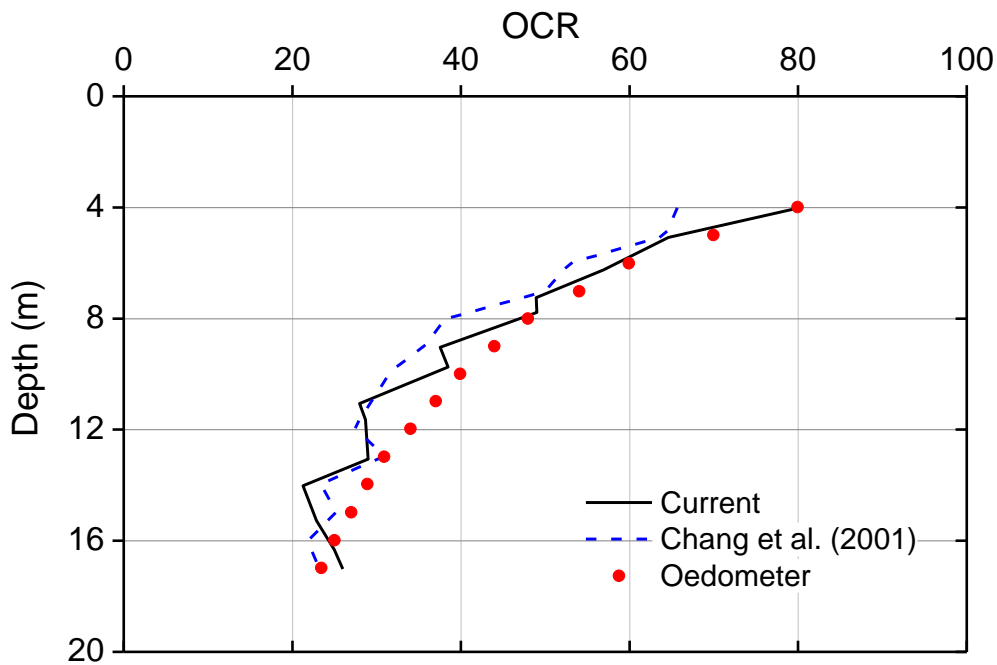


Fig. 10. Variation of OCR with depth

The variation of overconsolidation ratio with depth using the current solution is schematically presented in black solid line in Fig. 8, as well as the oedometer testing results and the interpretations from Chang et al. (2001), which, respectively, are shown in red solid circle and blue dash line. It shows that within the depth from 4 to 11 m, the current interpretation method presents the overconsolidation ratios that fit better with the oedometer test than Chang et al. (2001).

Even though at the depth of 11-16 m the predicted overconsolidation ratios by the current interpretation method deviates from the oedometer test, there are insignificant differences between them. In addition, at such depth the current interpretation method gives the overconsolidation ratios similar in magnitude to Chang et al. (2001). Hence, it is safe to say that the current interpretation method is effective in interpreting the properties of soil at Brent.

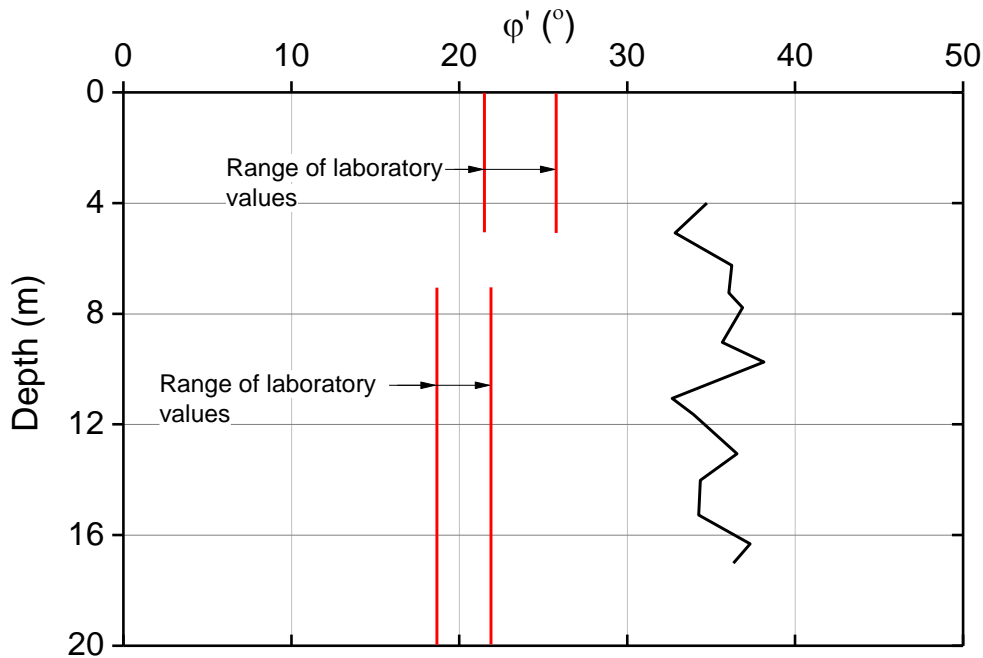


Fig.11. Variation of effective internal friction angle with depth

Fig. 11 shows the variation of the predicted effective internal friction angle ϕ' with depth as well as the value range of ϕ' provided by the laboratory test. It shows that the current interpretation method overestimates the effective internal friction angle throughout the whole depth. At the depth of 4 to 5 m, approximate 8° (30% overestimation) exists in the current interpretation method and the suggested value range of laboratory. Within the depth of 7 to 17 m, the suggested value range becomes narrow, and the current interpretation method produces the values of ϕ' that are about 12° (50% overestimation) higher than the laboratory values. Hence,

a conclusion can be drawn that the predicted φ' is in fairly good agreement with the laboratory values.

4.3.2. CPTu Test at Grangemouth

Geological records of prior soil borings indicated that the depth from 1 to 3 m was made of soft finely fissured dark grey veined light grey organic very silty clay with occasional fine to medium shell fragments; the depth from 3 to 5 m mainly included soft firm fissured black organic very silty clay with some small pockets of light brown silty clay; the depth from 6 to 8 m was soft intact dark grey black very organic silty clay with some brown veining; the depth of 9 to 10 m had soft slightly fissured black veined mid-brown organic silty clay; the depth of 11 to 12 m included soft firm vertically fissured black organic silty clay; from the depth of 13 to 15 m, it mainly had soft slightly fissured black veined mid-brown silty clay; below the depth of 15 m, the geomaterials were mainly firm strongly fissured dark grey slightly organic silty clay with some very small pockets and thin partings of light brown silty fine sand. The density of the soils at testing site was around 1650 kg/m^3 .

This test adopted a 10cm^2 cone with the penetration speed of 20mm/s. Powell et al. (1988) recommended the effective area ratio of $a = 0.7\sim 0.8$ to correct the measured cone tip resistance q_c . In this case study, $a = 0.75$ is used.

The obtained CPTu profile is shown in Fig. 12 below

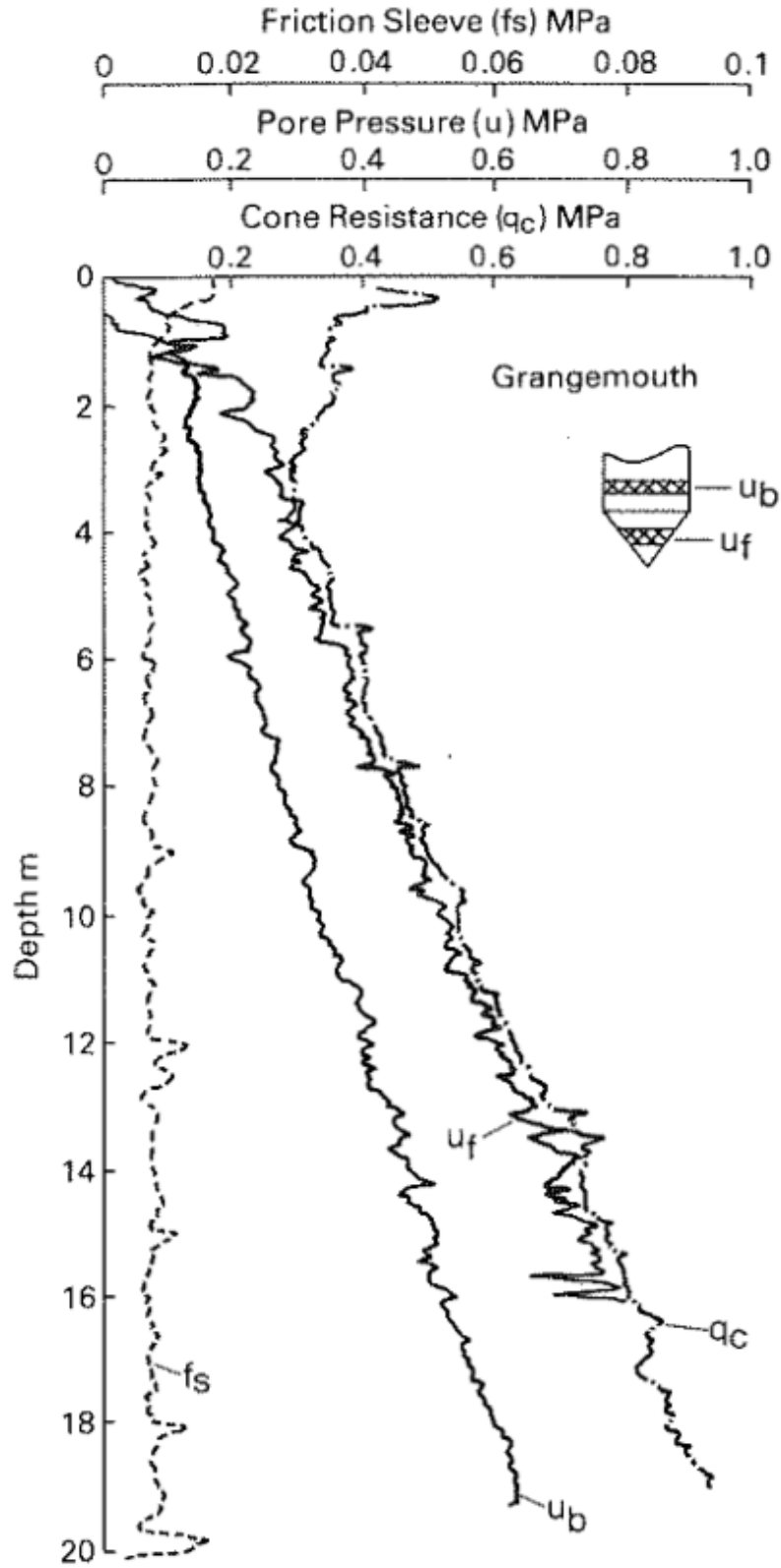


Fig.12. Typical Piezocone Profiles at Grangemouth (after Powell et al., 1988)

For the same reason, pore water pressure u_{bs} is obtained by multiplying a coefficient of 0.7 to the values of pore water pressure u_{bt} (Larsson and Mulabdic, 1991).

The variations of the overconsolidation ratios with depth predicted by the current interpretation method and the oedometer test are shown in Fig. 13. At the depth from 4 to 6 m, the current interpretation method slightly overestimates the overconsolidation ratios with the maximum deviation being around 0.6. Below the depth of 6.5 m, the current interpretation method underestimates the overconsolidation ratios of the soils slightly. The difference in value between these two curves is approximate 0.4. Based on the above analysis, it clearly indicates that the current interpretation method produces fairly good results with the experimental ones, even though some differences are seen between these two curves. Therefore, the current interpretation method can be said to be effective in predicting the stress history of the soils at Grangemouth site.

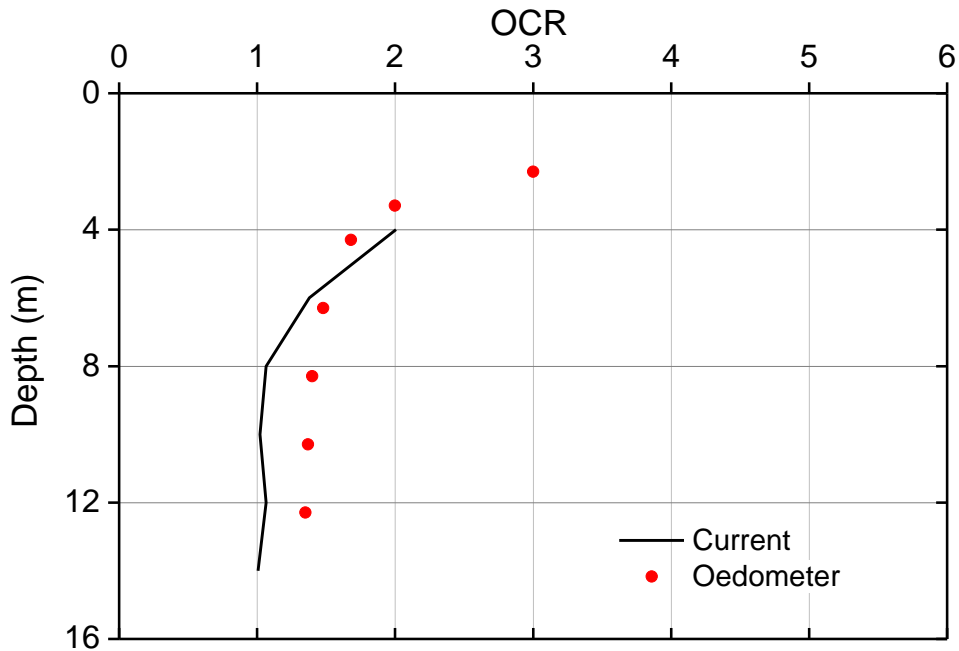


Fig. 13. Variation of OCR with depth

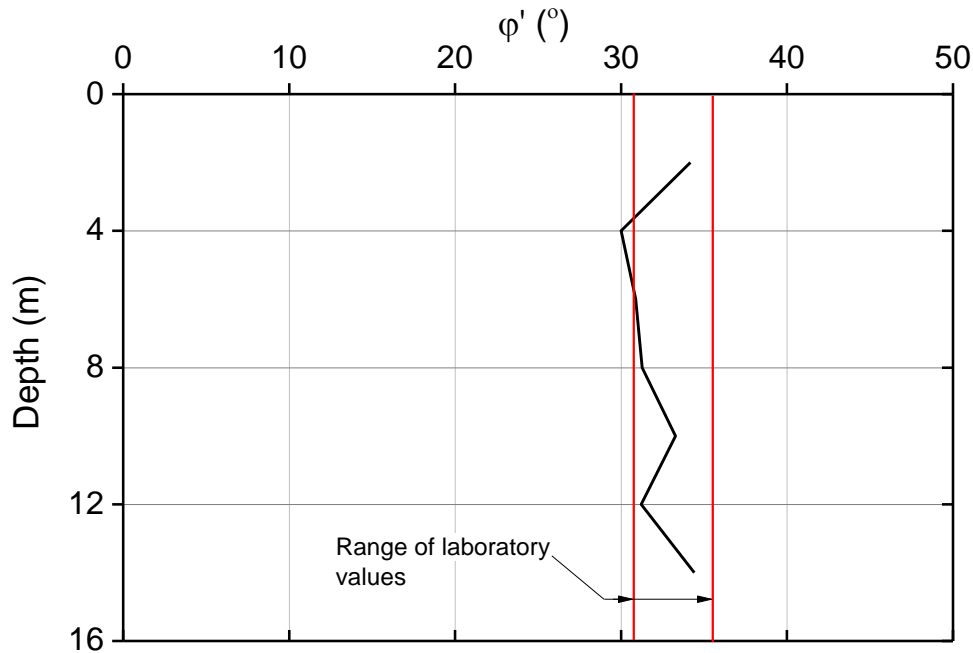


Fig. 14. Variation of effective internal friction angle with depth

Fig. 14 shows the variation of predicted effective internal friction ϕ' with depth as well as the value ranges of ϕ' provided by the laboratory. It shows that the current interpretation method generates the predicted ϕ' s that almost all lie in the value range suggested by the laboratory. The values of the predicted ϕ' s are around 33° . Therefore, the current interpretation method can be used to well interpret the properties of soils at Grangemouth.

4.4. Summary

Based on spherical and cylindrical cavity theories that, respectively, capture the penetration mechanism at cone face and friction sleeve sections, an interpretation model for the back-calculation of the properties of soil has been proposed. As illustrative examples, two testing sites have been interpreted using this interpretation model. The results indicate that at both Brent and Grangemouth sites, the predicted OCRs generally fit well with those from oedometer tests. It is also found that the interpretation model produces the effective internal friction angles within the

value range of laboratory test at Grangemouth site, although the effective internal friction angles at Brent site are overestimated by the current interpretation method and the back-calculated values are lying outside the value range of laboratory test. Generally, the interpretation model proposed in this report is able to interpret the properties of soil well.

CHAPTER 5. DEVELOPMENT OF INTERPRETATION SIMULATOR

5.1. Overview

It reveals that spherical cavity expansion theory can be applied to well describe the response of the soil around cone face during piezocone penetration test, while the friction sleeve has a penetration mechanism quite similar to cylindrical cavity expansion. Based on cavity theory and modified Cam Clay model, an interpretation method is proposed in this report, upon which the properties of soil, e.g., undrained shear strength, slope of critical state line in $p' - q$ plane, and the overconsolidation ratio, are able to be calculated in a straightforward manner using the explicit equations (4.10), (4.12.a), and (4.14), respectively. Considering that solving the above equations will not be difficult at all, this report will conduct the back-calculation with the use of Mathematica, a very common software in engineering.

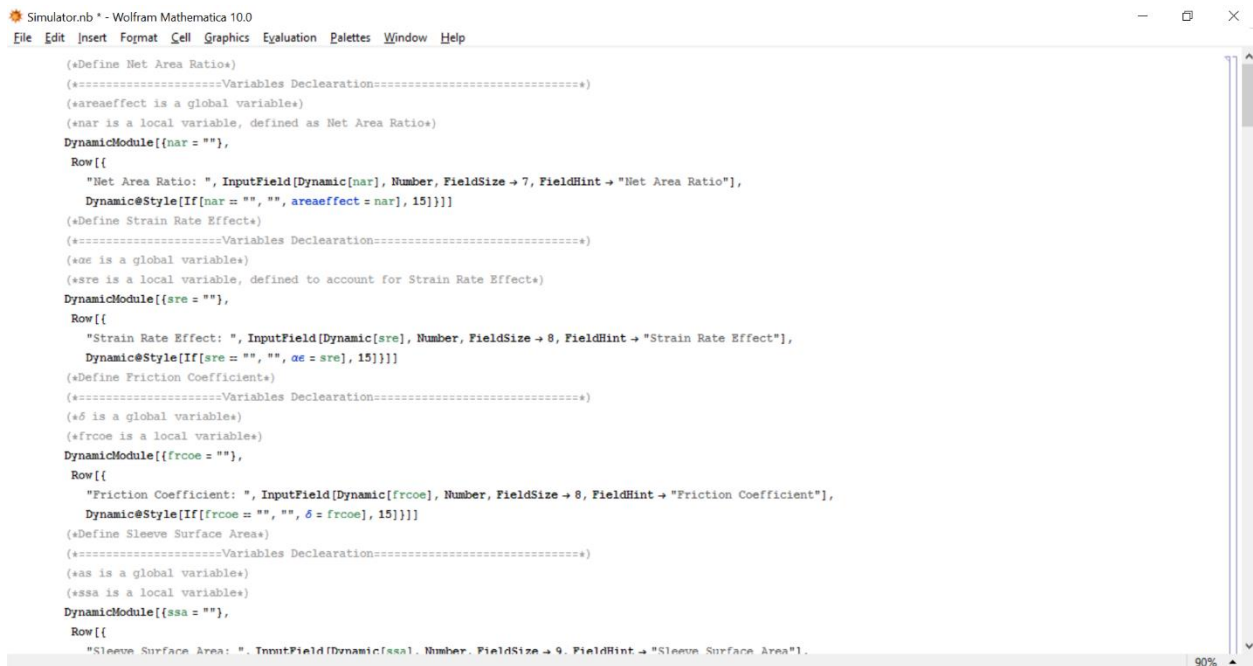
5.2. Mathematica Introduction

Mathematica, developed by Wolfram Research of Champaign Illinois, is a mathematical symbolic computational program that can be used in scientific, engineering, mathematical, and computing fields. In recent years, the capabilities for high-performance computing have been significantly extended with the introduction of packed arrays and sparse matrices, and by adopting the GNU Multi-Precision Library to evaluation high-precision arithmetic. In addition, Mathematica is of user-friendly since its programming language is so straightforward. For example, the expression of $y^2 = x^2 + 1$ can be directly written into Mathematica notebook for the purpose of calculating y , even without changing the form and format of the expression.

5.3. Program Usage

The current interpretation model is programmed on the platform of Mathematica 11.0 using its built-in Wolfram Language. To run this model, users need to install the same or higher versions of Mathematica.

After opening the *.nb file of the current interpretation model, the main interface will be shown below.



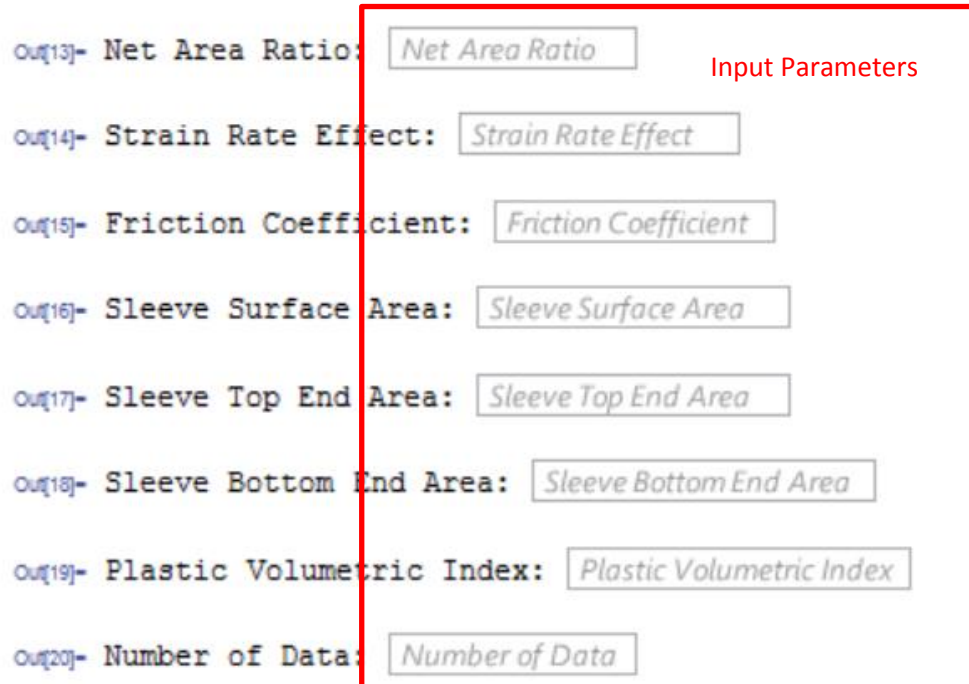
```
 Simulator.nb * - Wolfram Mathematica 10.0
File Edit Insert Format Cell Graphics Evaluation Palettes Window Help

(*Define Net Area Ratio*)
(=====Variables Declaration=====)
(*areaeffect is a global variable*)
(*nar is a local variable, defined as Net Area Ratio*)
DynamicModule[{nar = ""},
Row[{
  "Net Area Ratio: ", InputField[Dynamic[nar], Number, FieldSize -> 7, FieldHint -> "Net Area Ratio"],
  Dynamic@Style[If[nar == "", "", areaeffect = nar], 15]]]}]
(*Define Strain Rate Effect*)
(=====Variables Declaration=====)
(*ae is a global variable*)
(*sre is a local variable, defined to account for Strain Rate Effect*)
DynamicModule[{sre = ""},
Row[{
  "Strain Rate Effect: ", InputField[Dynamic[sre], Number, FieldSize -> 8, FieldHint -> "Strain Rate Effect"],
  Dynamic@Style[If[sre == "", "", ae = sre], 15]]]}]
(*Define Friction Coefficient*)
(=====Variables Declaration=====)
(*delta is a global variable*)
(*frcoe is a local variable*)
DynamicModule[{frcoe = ""},
Row[{
  "Friction Coefficient: ", InputField[Dynamic[frcoe], Number, FieldSize -> 8, FieldHint -> "Friction Coefficient"],
  Dynamic@Style[If[frcoe == "", "", delta = frcoe], 15]]]}]
(*Define Sleeve Surface Areas*)
(=====Variables Declaration=====)
(*sas is a global variable*)
(*ssa is a local variable*)
DynamicModule[{ssa = ""},
Row[{
  "Sleeve Surface Area: ", InputField[Dynamic[ssa], Number, FieldSize -> 9, FieldHint -> "Sleeve Surface Area"]
}]}]
```

Fig. 15. Main interface

The developed calculation program is easy for use, as interactive interfaces are automatically shown during the code running to indicate that specific parameters are required. The input parameters in the program include the those of CPTu tool itself, such as the effective area ratio α , the coefficient of friction δ between the penetrometer and the tested soil, the surface area of sleeve A_s , and the top and bottom end areas of sleeve A_{bt} and A_{bs} (Fig. 16). In addition, the field measured data is required, such as cone tip resistance q_c , sleeve friction f_s , pore pressure

measurements u (u_1 is the pore pressure at cone tip; u_2 is the pore pressure behind cone tip; u_3 is the pore pressure behind friction sleeve), and the burial depth h (Fig. 17).



The image shows a software interface with a list of input parameters. Each parameter is followed by a text input field. A red rectangular box highlights the entire list of parameters and their input fields. To the right of the first parameter, the text 'Input Parameters' is written in red.

- 0.4[13]- Net Area Ratio:
- 0.4[14]- Strain Rate Effect:
- 0.4[15]- Friction Coefficient:
- 0.4[16]- Sleeve Surface Area:
- 0.4[17]- Sleeve Top End Area:
- 0.4[18]- Sleeve Bottom End Area:
- 0.4[19]- Plastic Volumetric Index:
- 0.4[20]- Number of Data:

Fig. 16. Interactive interface requiring parameters of CPTu tool and other basic ones

0419- Data No.1:

cone tip resistance sleeve friction cone tip pore pressure cone base pore pressure behind sleeve pore pressure depth

Data No.2:

cone tip resistance sleeve friction cone tip pore pressure cone base pore pressure behind sleeve pore pressure depth

Data No.3:

cone tip resistance sleeve friction cone tip pore pressure cone base pore pressure behind sleeve pore pressure depth

Data No.4:

cone tip resistance sleeve friction cone tip pore pressure cone base pore pressure behind sleeve pore pressure depth

Data No.5:

cone tip resistance sleeve friction cone tip pore pressure cone base pore pressure behind sleeve pore pressure depth

Data No.6:

cone tip resistance sleeve friction cone tip pore pressure cone base pore pressure behind sleeve pore pressure depth

Input Parameters

Results: Su = M = OCR = φ =

Results: Su = M = OCR = φ =

Results: Su = M = OCR = φ =

Results: Su = M = OCR = φ =

Output Parameters

Fig. 17. Interactive interface requiring field measured data

After assigning values to the blanks in Figs. 16-17 as required by the developed interactive interface, the soil's properties, such as undrained shear strength s_u , slope of critical state line in $p' - q$ plane M , and the overconsolidation ratio OCR , are able to be determined immediately. Figs. 18-19 demonstrates the interface filled out with data and the obtained properties of soil.

Out[1]- Net Area Ratio: 0.75
Out[2]- Strain Rate Effect: 1.64
Out[3]- Friction Coefficient: 0.8
Out[4]- Sleeve Surface Area: 150.2
Out[5]- Sleeve Top End Area: 2.5
Out[6]- Sleeve Bottom End Area: 2.5
Out[7]- Plastic Volumetric Index: 0.75
Out[8]- Number of Data: 7

Fig. 18. Interactive interface filled out with parameters of CPTu tool and other basic ones

Data No.1:	3.0273	0.126686; 101	1.2092	-0.02256	-0.015792	13.06	Results:	Su = 0.676384	M = 1.48556	OCR = 28.9733
Data No.2:	2.4864	0.160926; 21	1.0698	-0.02324	-0.016268	11.06	Results:	Su = 0.494617	M = 1.3167	OCR = 27.9825
Data No.3:	cone tip resistance	sleeve friction	cone tip pore pressure	cone base pore pressure	behind sleeve pore pressure	depth	Results:	Su =	M =	OCR =
Data No.4:	cone tip resistance	sleeve friction	cone tip pore pressure	cone base pore pressure	behind sleeve pore pressure	depth	Results:	Su =	M =	OCR =
Data No.5:	cone tip resistance	sleeve friction	cone tip pore pressure	cone base pore pressure	behind sleeve pore pressure	depth	Results:	Su =	M =	OCR =
Data No.6:	cone tip resistance	sleeve friction	cone tip pore pressure	cone base pore pressure	behind sleeve pore pressure	depth	Results:	Su =	M =	OCR =

Fig. 19. Interactive interface with obtained properties of soil

5.4. Summary

On the basis of the explicit equations (4.10), (4.12.a), and (4.14), this chapter presents an interpretation model to interpret the properties of soil, such as undrained shear strength, slope of critical state line in $p' - q$ plane, and the overconsolidation ratio, with the use of Mathematica 11.0. To facilitate the calculation, an user-friendly interface is developed where users are required to input the CPTu measurements and some essential parameters of CPTu tool itself. A basic introduction to the program has been made, and an instruction about the program has been elaborated with necessary examples.

CHAPTER 6. CONCLUDING REMARKS

6.1. Conclusions

There are various methods available now to interpret the results of piezocone penetration test. However, most of the interpretation equations and correlation coefficients/parameters relating the soil characteristics to the CPTu data are largely empirical in nature and/or often based on over simplistic formulations, thus lacking the analytical rigor from the theoretical point of view. This study aims at interpretation of CPTu testing in a theoretical and rigorous manner.

On the basis of modified Cam Clay model, this report proposes an exploratory study on the application of the derived exact elastoplastic solutions for cavity problems to the interpretation of and maximum benefit extraction from the piezocone penetration tests. Studies have shown that during CPTu test, the penetration of a cone produces displacements that are quite similar to those developed during the expansion of a cavity. To be specific, the penetration at cone face section has been found to be similar to expand an existing spherical cavity from the current radius to infinity, whereas the penetration at friction sleeve section to be well explained using cylindrical cavity theory. Therefore, this report aims to combine both spherical and cylindrical cavity theories simultaneously to interpret the properties of soil from CPTu testing profiles.

Here, it has to be mentioned that this study is an exploratory and pilot one due to its rigorous interpretation of the properties of soil from CPTu testing, and more importantly to the inclusion of one more factor, i.e., sleeve friction, into the framework of the current interpretation model. Compared with previous studies (Chang et al., 2001; Zhang et al., 2016), this interpretation model attempts to take advantage of more information obtained from CPTu testing and expects to determine the properties of soil in an accurate way.

In this report, the exact solutions under spherical and cylindrical conditions for the ultimate state have been proposed. Based on these exact solutions and the relevant expertise of CPTu test, an interpretation model used to extract the properties of soil from CPTu testing profiles has been developed. Thereafter, two case studies have been conducted with the current interpretation model. The results indicate that the interpretation model is able to interpret well the overconsolidation ratios at both Brent and Grangemouth sites. For the effective internal friction angle, even though the predicted values at Brent site have been overestimated with the maximum error of 50%, the generated results at Grangemouth by the current interpretation model fits well with those from oedometer test. Therefore, the proposed interpretation model generally is effective in the prediction of the properties of soil.

6.2. Suggestions and Further Research

Future research is suggested as follows:

(1) For Brent site, the back-calculation results fit well with the oedometer testing results only when the strain rate $\alpha_\varepsilon = 2.7$; for Grangemouth site, α_ε needs to take the value of 2.85. However, Chang et al. (2001) suggested that α_ε should take a value around 1.63. Such difference in the value of α_ε between the current study and Chang et al. (2001) may arise from the assumption that only the spherical undrained shear strength $s_{u,S}$ is corrected by α_ε with friction sleeve section uncorrected; and

(2) The currently developed simulation framework is based on the symbolic computational software Mathematica. Given the explicit nature of the derived relationships between soil properties and CPTu measurements, such a Mathematica platform-based simulator development, rather than upon the Fortran and DLL files as originally planned in the proposal, is found sufficient

to realize the proposed interpretation approach. The adoption of Fortran codes together with DLL files will be considered by the research team in the future work, when the element of excess pore pressure at cone face is fully implemented into the interpretation method.

REFERENCES

- Baligh, M. M. (1985). Strain path method. *Journal of Geotechnical Engineering*, 111, No. 9, 1108–1136.
- Baligh, M. M. (1986). Undrained deep penetration: II. Pore Pressures. *Géotechnique*, 36, No. 4, 487–501.
- Battaglio, M., Bruzzi, D., Jamiolkowski, M. and Lancellotta, R. (1986). Interpretation of CPTs and CPTUs, 1st part: undrained penetration of saturated clays. *Proc. 4th Int. Geotech. Sem. Field Instrumentation and In-Situ Measurements*, Singapore. 129-143.
- Broms, B.B. and N. Flodin, (1988). History of Soil Penetration Testing, *Proceedings of the First International Symposium on Penetration Testing*, Vol. 1, Orlando (Penetration Testing 1988, Balkema, Rotterdam), March 20-24, pp, 157-220.
- Cai, G. J., Liu, S. Y., Tong, L. Y., and Du, G. Y. (2009). Assessment of Direct CPT and CPTU methods for predicting the ultimate bearing capacity of single piles. *Eng. Geol*, **104**(1): 211-222.
- Cai, G., Zou, H., Liu, S., et al. (2017). Random field characterization of CPTU soil behavior type index of Jiangsu quaternary soil deposits. *Bulletin of Engineering Geology and the Environment*, 76, No. 1: 1-17.
- Campanella, R.G., Gillespie, D. and Robertson, P.K. Pore pressure during cone penetration testing. *Proc. 2nd European Symp. On Penetration Testing*, Amsterdam, May 1982, Vol II, 507-512.
- Cao, L. F., Teh, C. I., and Chang, M. F. (2001). Undrained cavity expansion in modified Cam clay I: Theoretical analysis. *Géotechnique*, **51**(4): 323-334.
- Carter, J.P., Booker, J.R., and Yeung, S.K. (1986). Cavity expansion in cohesive frictional soils. *Geotechnique*, **36**(3): 349-358.

- Chang, M. F., Teh, C. I., and Cao, L. F. (2001). Undrained cavity expansion in modified Cam clay II: Application to the interpretation of the piezocone test. *Geotechnique*, **51**(4): 335-350.
- Chen, B.S. (1994). *Profiling stress history of clays using piezocone tests with dual pore pressure measurements*. PhD thesis, Georgia Institute of Technology, Atlanta, GA.
- Chen, S.L. and Absouleiman, Y.N. (2012). Exact undrained elasto-plastic solution for cylindrical cavity expansion in modified Cam Clay soil. *Geotechnique*, **62**(5): 447-456.
- Ching, J. Y., Phoon, K. K., Chen, C. H, et al. (2014). Modeling piezocone cone penetration (CPTU) parameters of clays as a multivariate normal distribution. *Canadian Geotechnical Journal*, 51, No. 1, 77-91.
- DeRuiter, J. (1971). Electric Penetrometer for Site Investigations., *Journal of the Soil Mechanics and Foundations Division* (ASCE), 97, SM2, 457-472.
- Durgunoglu, H. T., and Mitchell, J. K. (1973). Static penetration resistance of soils. *Proceedings of Special Conference on In-Situ Measurement of Soil Properties*, ASCE, New York, N.Y., Vol. I, pp, 151-189.
- Eslami, A., Fellenius, B. H. (1997). Pile capacity by direct CPT and CPTU methods applied to 102 case histories. *Canadian Geotechnical Journal*, 34 No. 6, 886-904.
- Jamiolkowski, M., Ladd, C.C., Germaine, J.T. and Lancellotta, R. (1985). New developments in field and laboratory testing of soils. *Proc. 11th Int. Conf. on Soil Mech. and Found. Engng*, San Francisco **1**, 57-153.
- Konrad, J.M. and Law, K.T. (1987). Preconsolidation pressure from piezocone tests in marine clays. *Geotechnique*. **37**(2): 177-190.

- Lacasse, S. and Lunne, T. (1982). Penetration tests in two Norwegian clays. *Proc. 2nd Eur. Symp. Penetration Testing*, Amsterdam **2**, 661-669.
- Lunne, T., Eidsmoen, T.E., Gillespie, D. and Howland, J.D. (1986). Laboratory and field evaluation of cone penetrameters, *Proceedings of the ASCE specialty conference on use of in situ tests in geotechnical engineering*, Blacksburg, Virginia, pp. 714-729.
- Mayne, P. W. (1991). Determination of OCR in Clays by Piezocone Tests Using Cavity Expansion and Critical State Concepts. *Soils Found.*, **31**(4): 65-76.
- Powell, J.J.M., Quarterman, R.S.T. and Lunne, T. (1988). Interpretation and use of the piezocone test in UK clays. In *penetration testing in the UK*, pp. 151-156. London: Thomas Telford.
- Rad, N.S. and Lunne, T. (1988). Direct correlations between piezocone test results and undrained shear strength of clay. *Proc. 1st Int. Symp. Penetration Testing*, Orlando **2**, 911-917.
- Robertson, P. K. (2009). Interpretation of cone penetration tests-a unified approach. *Canadian Geotechnical Journal*, 46, No. 11, 1337-1355.
- Senneset, K., (1974). Penetration Testing in Norway, Proceedings of the European Symposium on Penetration Testing, Vol. 1, Swedish Geotechnical Society, Stockholm, June 5-7, pp, 85-95.
- Sully, J. P., Campanella, R. G., Robertson, P. K., et al. (1988). Overconsolidation ratio of clays from penetration pore pressures. *Journal of Geotechnical Engineering*, 114, No. 2, 209-216.
- Teh, C. I., and Houlsby, G. T. (1991). An analytical study of the cone penetration test in clay. *Geotechnique*, **41**(1): 17-34.
- Timoshenko, S.P. and Goodier, J.N. (1970). *Theory of elasticity*. New York: McGraw-Hill.
- Vesic, A. S. (1972). Expansion of cavities in infinite soil masses. *Journal of Soil Mechanics Found Division ASCE* 98, No.3, 265-290.

Wood, D.M. (1990). *Soil behavior and critical state soil mechanics*. Cambridge: Cambridge University Press.

Yu, H.S. (2000). *Cavity expansion methods in geomechanics*. Dordrecht: Kluwer Academic.

Zhang, Y., Li, J. Liang, F., and Tang, J. (2016). Interpretation of cone resistance and pore-water pressure in clay with a modified spherical cavity expansion solution. *Bul. Eng. Geol. Environ.*, **75**(1): 391-399. DOI: 10.1007/s10064-015-0732-y.

APPENDIX

The code for the interpretation model is presented below.

(*Define Net Area Ratio*)

(*=====VariablesDeclearation=====*)

(*areaeffect is a global variable*)

(*nar is a local variable, defined as Net Area Ratio*)

DynamicModule[{nar = ""},

Row[{

 "Net Area Ratio: ",

 InputField[Dynamic[nar], Number, FieldSize -> 7,

 FieldHint -> "Net Area Ratio"],

 Dynamic@Style[If[nar == "", "", areaeffect = nar], 15]]]

(*Define Strain Rate Effect*)

(*=====Variables Declearation=====*)

(* $[\text{Alpha}][\text{Epsilon}]$ is a global variable*)

(*sre is a local variable, defined to account for Strain Rate Effect*)

```
DynamicModule[{sre = ""},
```

```
Row[{
```

```
  "Strain Rate Effect: ",
```

```
  InputField[Dynamic[sre], Number, FieldSize -> 8,
```

```
    FieldHint -> "Strain Rate Effect"],
```

```
  Dynamic@Style[If[sre == "", "",  $\alpha$ [Epsilon] = sre], 15]]]
```

```
(*Define Friction Coefficient*)
```

```
(*=====Variables Decleration=====*)
```

```
(* $\Delta$  is a global variable*)
```

```
(*frcoe is a local variable*)
```

```
DynamicModule[{frcoe = ""},
```

```
Row[{
```

```
  "Friction Coefficient: ",
```

```
  InputField[Dynamic[frcoe], Number, FieldSize -> 8,
```

```
    FieldHint -> "Friction Coefficient"],
```

```
  Dynamic@Style[If[frcoe == "", "",  $\Delta$  = frcoe], 15]]]
```

```
(*Define Sleeve Surface Area*)
```

(*=====Variables Declearation=====*)

(*as is a global variable*)

(*ssa is a local variable*)

DynamicModule[{ssa = ""},

Row[{

 "Sleeve Surface Area: ",

 InputField[Dynamic[ssa], Number, FieldSize -> 9,

 FieldHint -> "Sleeve Surface Area"],

 Dynamic@Style[If[ssa == "", "", as = ssa], 15]]]

(*Define Sleeve Top End Area*)

(*=====Variables Declearation=====*)

(*abs is a global variable*)

(*stea is a local variable*)

DynamicModule[{stea = ""},

Row[{

 "Sleeve Top End Area: ",

InputField[Dynamic[stea], Number, FieldSize -> 9,

FieldHint -> "Sleeve Top End Area"],

Dynamic@Style[If[stea == "", "", abs = stea], 15]]]

(*Define Sleeve Bottom End Area*)

(*=====Variables Decleration=====*)

(*abt is a global variable*)

(*sbea is a local variable*)

DynamicModule[{sbea = ""},

Row[{

"Sleeve Bottom End Area: ",

InputField[Dynamic[sbea], Number, FieldSize -> 10,

FieldHint -> "Sleeve Bottom End Area"],

Dynamic@Style[If[sbea == "", "", abt = sbea], 15]]]

(*Define Plastic Volumetric Index*)

(*=====Variables Decleration=====*)

(*\[CapitalLambda] is a global variable*)

(*pvi is a local variable*)

```
DynamicModule[{pvi = ""},
```

```
Row[{
```

```
  "Plastic Volumetric Index: ",
```

```
  InputField[Dynamic[pvi], Number, FieldSize -> 10,
```

```
    FieldHint -> "Plastic Volumetric Index"],
```

```
  Dynamic@Style[If[pvi == "", "", \[CapitalLambda] = pvi], 15]]]
```

(*Define Number of data*)

(*=====Variables Decleration=====*)

(*NN is a global variable*)

(*nod is a local variable*)

```
DynamicModule[{nod = ""},
```

```
Row[{
```

```
  "Number of Data: ",
```

```
  InputField[Dynamic[nod], Number, FieldSize -> 7,
```

```
    FieldHint -> "Number of Data"],
```

```
  Dynamic@Style[If[nod == "", "", NN = nod], 15]]]
```

```

ss2 = Table[
  {
    DynamicModule[{contipresis = "", slvfric = "",
      contipporpress = "", conbaseporpress = "",
      behfricsleevporpress = "", burialdepth = ""},
    Row[{
      "Data No.", k, ": ",
      InputField[Dynamic[contipresis], Number, FieldSize -> 5,
        FieldHint -> "cone tip resistance"], " ",
      InputField[Dynamic[slvfric], Number, FieldSize -> 5,
        FieldHint -> "sleeve friction"], " ",
      InputField[Dynamic[contipporpress], Number, FieldSize -> 5,
        FieldHint -> "cone tip pore pressure"], " ",
      InputField[Dynamic[conbaseporpress], Number, FieldSize -> 5,
        FieldHint -> "cone base pore pressure"], " ",
      InputField[Dynamic[behfricsleevporpress], Number,
        FieldSize -> 5, FieldHint -> "behind sleeve pore pressure"],
      " ",
      InputField[Dynamic[burialdepth], Number, FieldSize -> 5,

```

FieldHint -> "depth"], " Results: Su = ",

Dynamic@

Style[If[

contipresis == "" || slvfric == "" || contipporpress == "" ||

conbaseporpress == "" || behfricsleevporpress == "" ||

burialdepth == "", "",

sus = ((contipresis + (1 - areaeffect) conbaseporpress) -

contipporpress - (slvfric + (behfricsleevporpress abs -

conbaseporpress abt)/as)^[Delta]/(4/

3 \[Alpha]\[Epsilon] - 2/Sqrt[3]), 15], " M = ",

Dynamic@

Style[If[

contipresis == "" || slvfric == "" || contipporpress == "" ||

conbaseporpress == "" || behfricsleevporpress == "" ||

burialdepth == "", "",

CSLM = 2/((contipresis + (1 - areaeffect) conbaseporpress -

contipporpress)/(((contipresis + (1 -

areaeffect) conbaseporpress) -

contipporpress - (slvfric + (behfricsleevporpress \

abs - conbaseporpress abt/as)^[Delta]/(4/3 \[Alpha][Epsilon] -

2/Sqrt[3])) - 4/3], 15], " OCR = ",

Dynamic@

Style[If[

contipresis == "" || slvfric == "" || contipporpress == "" ||

conbaseporpress == "" || behfricsleevporpress == "" ||

burialdepth == "", "",

OCR = 2 ((2 (((contipresis + (1 -

areaeffect) conbaseporpress) -

contipporpress - (slvfric + (behfricsleevporpress \

abs - conbaseporpress abt/as)^[Delta]/(4/3 \[Alpha][Epsilon] -

2/Sqrt[

3]))/(2/((contipresis + (1 -

areaeffect) conbaseporpress -

contipporpress)/(((contipresis + (1 -

areaeffect) conbaseporpress) -

contipporpress - (slvfric + (behfricsleevporpress \

abs - conbaseporpress abt/as)^[Delta]/(4/3 \[Alpha][Epsilon] -

```

                2/Sqrt[3])) - 4/3)) (19.2 - 9.81) burialdepth/
                1000))^(1/[CapitalLambda]), 15],
"      \[CurlyPhi] = ",
Dynamic@
Style[If[
    contipresis == "" || slvfric == "" || contipporpress == "" ||
    conbaseporpress == "" || behfricsleevporpress == "" ||
    burialdepth == "", "",
    fai /. NSolve[
        2/((contipresis + (1 - areaeffect) conbaseporpress -
            contipporpress)/((contipresis + (1 -
            areaeffect) conbaseporpress) -
            contipporpress - (slvfric + (behfricsleevporpress \
abs - conbaseporpress abt)/as)^[Delta])/(4/3 \[Alpha]\[Epsilon] -
            2/Sqrt[3])) - 4/3) == (6 Sin[fai/360 2 Pi])/(
            3 - Sin[fai/360 2 Pi]), fai][[1, 1]], 15]
    ]}
, {k, 1, NN}];

```

Row[Table[ss2[[j, 1]], {j, 1, NN}]]

OUTCOMES

Publications (TIRE Award acknowledged)

Chen, S. L., and Liu, K. (2018). Undrained cylindrical cavity expansion in anisotropic critical state soils. *Geotechnique*, accepted.

Chen, S. L., and Abousleiman, Y. N. (2018). Cavity expansion in strain hardening frictional soils under drained condition. *International Journal for Numerical and Analytical Methods in Geomechanics*, 42: 132–142.

Chen, S. L., and Abousleiman, Y. N. (2017). Wellbore stability analysis using strain hardening and/or softening plasticity models. *International Journal of Rock Mechanics and Mining Sciences*, 93: 260-268.